MULTISCALE MODELING OF TARGETED DRUG DELIVERY

AND DIEP FLAP PERFUSION

by

MANOHARA MARIYAPPA

Presented to the Faculty of the Graduate School of

The University of Texas at Arlington in Partial Fulfillment

of the Requirements

for the Degree of

MASTER OF SCIENCE IN MECHANICAL ENGINEERING

THE UNIVERSITY OF TEXAS AT ARLINGTON

May 2010

ACKNOWLEDGEMENTS

I would like to express my deepest gratitude to my mentor Dr.Yaling Liu, for his constant suggestions, advice and encouragement throughout the course of my research without which this work could not have been accomplished. It is his knowledge, motivation and dedication that helped me to overcome the problems during trying times. I would also like to thank Professor Brian Dennis and Professor Kytai Nguyen for being a part of my committee. I appreciate Professor Nguyen and Soujanya for providing us the experimental results. I wish to express my warm and sincere thanks to all my lab mates for their continuous support in the lab. I am thankful to the staff at the Department of Mechanical and Aerospace Engineering at The University of Texas at Arlington for availing themselves to me at all times and supplying me with resources I never could have found without them.

Finally I would like to express my deepest appreciation to my parents and friends for their constant support during my research work.

April 16, 2010

ABSTRACT

MULTISCALE MODELING OF TARGETED DRUG DELIVERY

AND DIEP FLAP PERFUSION

Manohara Mariyappa, M.S.

The University of Texas at Arlington, 2010

Supervising Professor: Yaling Liu

Advances in computational techniques have changed diagnosis and treatment of chronic diseases. This thesis work is composed of developing computational models in two application areas: nanomedicine and determining DIEP flap perfusion for reconstructive surgery.

Nanomedicine poses a new frontier in medical technology with the advantages of targeted delivery and patient specific medicine. Current advances in nanomedicine are aiding the discovery and rationale design of many new classes of nanoparticles as drug delivery vectors for cancer treatment and image enhancing. An important advantage of targeted drug delivery is reduced drug dosage that enables the minimization of adverse effects associated with elevated drug concentrations. In applications of nanoparticle targeted drug delivery, the delivery efficiency is controlled by the physical properties of the nanoparticle such as its size, shape as well as external environmental conditions such as flow rate and blood vessel diameter. Proper drug dosage choice relies on determination of the attachment and detachment rates of nanoparticles and understanding the complex process of targeted drug delivery. A combined particulate and

continuum model is developed to understand the binding dynamics of nanoparticles under vascular conditions. The effect of shear rate, particle size and binding rates on bound density of nanoparticles is explored using the multiscale model. The developed multiscale model is expected to give insights into the complex drug delivery process.

Another aspect of the computational modeling is to determine the number and position of perforators for perfusion of Deep Inferior Epigastric artery Perforator (DIEP) flap for breast reconstructive surgery. DIEP is a tissue flap procedure that uses fat and skin from the abdomen to create a new breast mound after a mastectomy. A DIEP flap includes the movement of an artery and vein from the tissue flap to the chest so that the transplanted tissue can be supplied with blood. Usually additional perforators may be dissected and included with the flap for additional perfusion based on the size of the flap. The number and position of perforators play a vital role in keeping the tissue alive for successful reconstruction. The goal of this thesis work is to establish a numerical tool to determine the number of perforators as well as the position of perforators for optional perfusion based on specific vascular geometry.

TABLE OF CONTENTS

LIST OF ILLUSTRATIONS

Figure Page

LIST OF TABLES

Table Page

CHAPTER 1
INTRODUCTION

This thesis work consists of developing computational models in two application areas: targeted drug delivery and to determining perfusion of DIEP flap for breast reconstructive surgery. Targeted drug delivery involves modeling transportation and adhesion dynamics of functionalized nanoparticles onto receptor coated surface while DIEP flap perfusion model involves modeling a vascular network to optimize the number of perforators and the manner in which the perforators are connected for better perfusion of the flap. In this chapter, the backgrounds of the two applications are described separately.

1.1. Introduction to nanomedicine

A revolution in nanotechnology is pushing personalized cancer treatment and *in vivo* imaging closer than ever before. Nanomedicine has made advanced medical diagnosis and treatment possible which was once a subject of fiction and fantasy. The advantages of nanomedicine over conventional medicine are targeted drug delivery, sustained drug release, increased bio-availability, early cancer detection, chemotherapy of tuberculosis[4], minimal side effects and enhanced imaging[5] [6] [7] [8] [9] [10] [11]. The properties of nanoparticles, such as increased chemical activity and the ability to cross tissue barriers, are leading to new drug targeting and delivery techniques. Extensive studies have been devoted to study biological behavior of nanoparticles *in vivo* and *in vitro.* Most of the nanoparticle systems currently being studied are spherical in shape. For example, it is known that spherical particles bigger than 200 nm are efficiently filtered by the spleen, while particles smaller than 10 nm can be quickly cleared by the kidney, thus making 10-200 nm as the ideal size range for spherical carriers [12-13]. One of the advantages of nanoparticles is their size controllability. The efficiency of drug distribution in

various parts of the body is largely influenced by size [14] of the drug particles. By controlling the size of the particles, pharmacokinetic release of the drug can be controlled. Nanoparticles have to be designed in specific size for longer circulation in the blood stream. Gratton[15] et al studied the effect of particle size and aspect ratio on internalization kinetics of nanoparticles by HeLa cells. They demonstrated that cylindrical particles having diameters equal to 500 nm and 1 µm, both having heights of 1 µm, displayed similar internalization profiles, internalizing particles at a higher percentage (75%) than cubic-shaped 2µm particles (45%). One of the objectives of this work is to explore the effect of size[16] and binding rates on the binding dynamics of nanoparticles. Geng et al. [17] performed *in vivo* study to determine effect of size [18] on circulation of nanoparticles in the vascular network and demonstrated that spheres or short filomicelles are up taken by cells more easily than longer filaments [19]. This suggests that non-spherical particles have higher retention during circulation in blood vessel compared to their counterpart spherical ones. From these studies it is found that size of nanoparticles is a defining parameter in deciding the targeted drug delivery efficiency. Another aspect of this thesis is to study the effect of shear rate on nanoparticle adhesion dynamics. There has been extensive research to study the effect of shear rate [20] [21] [22] and nanoparticle size to understand the mechanism of targeted drug delivery. Haun et al [23] developed a continuum model to determine the effects of bound density and flow rate on adhesion of 210 nm particles. They also validated their continuum model with flow chamber experiments. They measured binding and detachment of particles in a flow chamber as a function of ligand density and flow rate. They used transport reaction model to determined binding rates. Takalkar et al[22] studied binding kinetics of micro bubbles under shear flow. They observed binding densities of micro bubbles under different shear rates and concluded that binding rate increases with shear rate. There have also been numerous *in vivo* studies to understand the nanoparticle adhesion dynamics. Farokhzad et al [6] conducted *in vitro* shear rate studies. They carried out experiments on attachment of nanoparticles on LNCaP cells under various shear rates. They demonstrated that at low shear stress less than 1.1 dyne/cm^2,

the average number of nanoparticle conjugates was more than 10 per cell while at shear stress of 4.5 dyne/cm^2 there was significant decrease (less than 1) in attachment of nanoparticles. However the effects of nanoparticle size and shear rate on binding dynamics have been seldom studied. The development of a wide spectrum of nanomedicine is beginning to change the foundations of disease diagnosis, treatment and prevention. These involve the identification of precise targets (cells and receptors) related to specific clinical conditions and choice of appropriate nanocarriers to achieve the required responses while minimizing the side effects. Mononuclear phagocytes, dendritic cells, endothelial cells, and cancers (tumor cells) are key targets[24]. Today, nanotechnology and nanoscience approaches to particle design and formulation are beginning to expand the market for many drugs and are forming the basis for a highly profitable niche within the industry. Indeed, research into the rational delivery and targeting of pharmaceutical, therapeutic, and diagnostic agents via intravenous and interstitial routes of administration with nanosized particles is at the forefront of projects in nanomedicine. However, one of the major hurdles and current problem in nanomedicine is to improve nanoparticle cell selectivity and adhesion efficiency through appropriate design of nanoparticles of various shapes, sizes and materials under vascular flow conditions.

Nanoparticle drugs to treat cancer are already in use, such as a liposome-encased version of the chemotherapy doxorubicin[25], as well as a variety of polymer drug combinations in which the drug and polymer molecules are meshed or chemically joined into nanoparticles (composites, conjugates, micelles, dendrimers). Some of the FDA approved nanoparticle based drugs available in the current market for treating different kinds of cancer are illustrated in Table 1 and figure 1. Doxil is used to treat AIDS-related Kaposi's sarcoma, breast cancer, ovarian cancer, and other solid tumors and Abraxane is used to treat breast cancer. Despite such advancements nanomedicine hasn't been widely used due to the lack of understanding of complex reaction processes and the physical properties of the particles which affect the drug delivery efficiency. Carrier design and targeting strategies vary in relation to the type,

development stage of the disease and the location of the disease. The next generation targeted particles bear additional features that increase their affinity for, and facilitate entry into, cancer cells.

Table 1 FDA approved nanoparticle based drugs in the market[25]

Particle Type	Product	Company	Treatment
Nanoparticle Albumin	Abraxane	Abraxis BioScience	Lung Cancer Breast Cancer
DNA functionalized gold nanoparticles	Verigene platform and bio-barcode technology	Nanosphere	Diagnosis
Doxorubicin liposome injection	Caelyx, Doxil	Ortho Biotech (Johnson & Johnson)	Recurrent breast cancer, ovarian cancer, AIDS related Kaposi's sarcoma
Liposome encapsulated doxorubicin citrate complex	Myocet	Zeneus Pharma	Recurrent breast cancer
Liposomal formulation of Daunorubicin	DaunoXome	Gilead Sciences	Kaposi's sarcoma

Figure 1 Nanoparticle based FDA approved drugs for cancer treatment in the market (Adapted from www.cvs.com and www.drugs.com).

1.2 Proposed work in nanomedicine

Mathematical models[26] [27]and simulation models [23] [28] [29]have been widely used in the past to study drug delivery mechanism. The computational methods will reduce the time and costs involved to develop a drug. Mathematical models that have been proposed so far to study nanoparticle adhesion kinetics are based on either equilibrium approach [30] [31]or kinetics approach [23]. Evans et al [31] have developed a continuum model to study binding dynamics of nanoparticles considering equilibrium forces required to separate adhesive contacts while Haun [23] et al considered binding and dissociation constants of the particles as a function of adhesion dynamics. We believe our research is the first attempt to integrate the particulate nature of the particle and the binding dynamics together in a continuum model.

Experimental procedures to understand nanoparticle targeting process is very challenging due to the interplay of transport, hydrodynamic force and multivalent bond formation dynamics. So a computational model is developed which can help to elucidate the underlying deposition mechanisms. To achieve dynamic process, a multiscale model of nanoparticle transport and adhesion dynamics is established. At the end, the developed model will be use to characterize the influence of nanoparticle size, receptor density and shear rate on bound density of nanoparticles. The proposed work is to develop a binding rate and particle size dependent unique multiscale computational convection-diffusion-reaction model that account for transport and adhesion phenomena. Also, effect of adhesion and detachment rates on binding of nanoparticles under shear flow will be explored. This research work will result in fundamental and in depth knowledge of transport and targeting efficiency of nanomedicine carriers, which will provide a new guidance to the design of nanomedicine for better treatment of diseases in general.

1.3. Background of DIEP flap

Over 200,000 new breast cancer cases are diagnosed annually in the United States alone [32]. When mastectomy is a part of the patient's treatment plan, women consider

immediate breast reconstruction. The DIEP (Deep Inferior Epigastric Perforator) flap procedure is the most advanced form of breast reconstruction surgery available today. DIEP flap for reconstructive surgery was first proposed by Koshima and Soeda [33]. Since then it has become an integral component in breast reconstructive surgery. It is the preferred reconstructive technique performed by surgeons. The surgery uses the patient's own abdominal tissue to reconstruct a natural, soft breast after mastectomy. The abdominal skin, fat and deep inferior epigastric vessels that supply necessary blood are removed and replanted to create a natural looking and aging breast. Figure 2 shows a typical DIEP flap with perforators dissected from the abdomen region. The abdominal wall tissue is characteristically similar to breast tissue, this can enhance the aesthetic outcome and make it a suitable donor for transplant. This procedure is carried out without sacrificing rectus abdominis muscle. Sparing these muscles decreases post surgical pain, expedites recovery and reduces patient's chance of developing a hernia or a bulge in the abdomen which are the usual complications that are associated with reconstructive problems that utilize the rectus muscle. Technical aspects of performing perforator flaps have been set forth by personal experience of surgeons who perform those surgeries routinely. It has been observed by surgeons that use of the largest perforator gives a better perfusion [34] as well as preference of incision of perforator. However, no theoretical or mathematical explanation has been proposed to support their observations. This research intends to help us choose ideal number of perforators and proper size of the flap. Another advanced aspect of this work is extracting vascular geometry from CT/MRI scanned images for determining perfusion in the flap through CFD simulations. The focus of this work is to develop a continuum model for determining optimum perforator configuration for successfully reconstructive surgery.

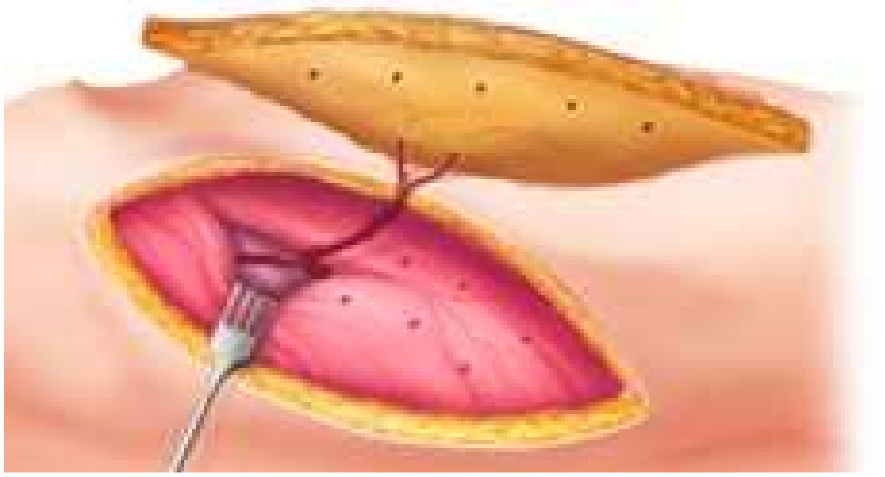

Figure 2 A perforator vessel connected to capillaries. (Adapted from http://microsurgeon.ca/perforator-flaps)

1.4 Proposed work in characterizing DIEP flap perfusion

The deep inferior epigastric perforator (DIEP) flap is based on the deep inferior epigastric vessels at the bottom of the rectus abdominis muscle. These vessels provide the primary blood supply to the skin and fat of the lower abdomen. In the DIEP flap, the lower abdominal skin and fat is removed without having to harvest any of the rectus abdominis muscle. Instead, blood supply is provided through the perforator vessels that are teased out from the rectus muscle, using a muscle incision alone. The surgeon will apply judgment in the operating room to determine how many perforators are needed to provide sufficient blood supply for the DIEP flap to survive which are prone to mistakes. If a DIEP procedure fails the tissue flap may die or have to be completely removed. The challenges associated with breast reconstruction using DIEP flap procedure include bleeding, fluid collection and blood profusion in the vasculature [35]. It is a critical issue to determine the number of perforators and the location of perforators to keep the tissue well perfused for successful transplant. Experimental studies to determine the flap perfusion and choosing ideal number of perforators require sacrificing human tissue. To overcome this disadvantage, a computational model is developed. Patel and Keller [36] developed a mathematical model based on physics of flow through vessels and the current-

resistance circuit analogy. They showed that the best perfused flap involves use of the largest diameter vessel. But they assumed that perforators are connected in parallel and did not address the interconnectivity of the vascular network. This thesis work consists of developing a computational model to determine the number of perforators for optimum perfusion of the flap. Also, a mathematical model similar to Keller and Patel model is developed based on the actual resistance of different blood vessels in the vascular network to support the results from the continuum model.

CHAPTER 2

MODELING TARGETED DRUG DELIVERY PROCESS

2.1 Introduction to targeted drug delivery

A long standing issue for drug delivery is to deliver the correct dose of a particular therapeutic drug to the specific disease site. Since this is generally unachievable from traditional methods, therapeutics have to be administered in excessively high doses, thereby increasing the odds of toxic side effects. The concept of site specific delivery of a therapeutic arises from this drawback of traditional therapeutics. In recent years, there has been a surge of interest in nanoparticle drug delivery systems in pharmacy. This is in part due to the advantages these systems provide over existing systems. Designing drug delivery system is challenging in terms of targeting the drug to specific sites. An appropriate method would be to develop a computational modeling technique, which incorporates fundamental physical principles that dictates dynamics of nanoparticle delivery and adhesion process. Quantitative analysis based on the developed continuum model will facilitate an optimum model of the drug delivery system to the researchers and support a rational framework for the cancer treatment research.

There have been several particulate models to study the binding dynamics of nanoparticles [37] [38]. Ferrari and Decuzzi [38] [21] studied effect of particle size and demonstrated that the number of particles binding to the cell layer per unit surface decreases with the size of the particle diameter. They also showed that there is an optimal particle size corresponding to the largest strength of adhesion. Therefore it is important to study the properties of nanoparticles that affect targeted drug delivery under vascular flow environment where particles are under constant shear stress. Nanoparticles usually enter the vascular circulation system through intravenous injection. The targeted delivery efficiency is directly related to

nanoparticle selectively and ability to bind at the targeted site. Though highly selective nanoparticles have reduced binding probability in non-target regions, the majority of nanoparticles are still lost in the vascular network due to non-specific adhesion. At the nanoscale, the binding dynamics of nanoparticles is a complex process which involves the interaction of blood which by itself is a complex fluid. There have been extensive studies to understand the nanoparticle binding dynamics at the particulate level. The focus of this work is to develop an integrated particulate and continuum model to study the nanoparticle adhesion dynamics. A multiscale framework integrating particulate model and continuum model is pursued to model the targeted drug delivery system.

2.2 Fundamental theories of targeted drug delivery

Targeted drug delivery is achieved via specific adhesion, where, nanoparticles are functionalized with polymers that bind specifically to a particular type of receptors on the cell surface; these receptors are exclusively expressed during certain disease state. The experimental study of nanoparticle flow *in vivo* is difficult due to complex vascular network, transport and chemical reactions involved. Computational models [20] [27] [23]provide a bridge for better understanding the complex processes involved. For example Decuzzi et al [39] have developed particulate model to study the shape and size of nanoparticles. Haun et al[23] studied the effect of shear rate and binding rates on the adhesion dynamics of nanoparticles in a transport reaction continuum model. But it has been observed that shear rate of blood flow in the vascular network affects the adhesion and detachment rates and hence the bound density of nanoparticles on the active site[38]. A coupled continuum model to study the transport and adhesion of nanoparticles is yet to be developed. The objective of our study is to develop a coupled particulate and continuum model to study the effect of size of nanoparticles and shear rate on the targeted delivery. We coupled the adhesion probability formulation of Decuzzi *et al* with continuum convection-diffusion-reaction model to study the influence of flow rate and particle

size on deposition of nanoparticle density. The simulated results are compared with experimental data.

2.3. Convection diffusion reaction model

A finite element model is developed to evaluate the nanoparticle transportation diffusion and biochemical reaction dynamics. In this model, the convection diffusion in the 2D fluid domain is coupled with the adhesion reaction occurring only on the reaction surface. The transport of nanoparticles in the vascular medium is defined by the convection-diffusion equation,

$$\frac{\partial c}{\partial t} + u \cdot \nabla c = D\nabla^2 c \qquad (2.3.1)$$

where c is the particle concentration, D is the particle diffusivity, u is the velocity in the axial direction. Particle diffusivity is calculated from the Stokes-Einstein equation for particles of different sizes [40].

$$D = \frac{k_B T}{6\pi\mu R} \qquad (2.3.2)$$

where μ is the viscosity of the fluid medium, R is the particle radius, T is the absolute temperature and k_B is Boltzmann's constant. The biorecognition of the targeted drug delivery site is like a key lock mechanism which is in reality a complex biochemical reaction. To incorporate the effect of adsorption of nanoparticles on a functionalized surface, Langmuir reaction model is used[41]. The chemical reaction is a weakly reversible process because the nanoparticles are constantly captured on the receptor surface and constantly detached [42]. The material balance for the active surface including surface diffusion and the reaction rate expression for the formation of the adsorbed species c_s is defined by:

$$\frac{\partial c_s}{\partial t} + \nabla \cdot (-D_s \nabla c_s) = k_a c\theta - k_d c_s \qquad (2.3.3)$$

Where D_s is the surface diffusivity, c is the bulk concentration of the species at surface, θ is the

surface concentration on the active site and c_s surface concentration of adsorbed species. k_a, k_d are adhesion and detachment rates respectively. However the concentration of active sites is equal to the difference between the total concentration of active sites and the number of sites occupied by the adsorbed species. This gives the equation for the reaction rate as

$$\frac{\partial c_s}{\partial t} + \nabla.(-D_s \nabla c_s) = k_a c(\theta_0 - c_s) - k_d c_s \qquad (2.3.4)$$

In the above equation θ_0 represents the total number of active sites available on the active surface. In our coupled particulate-continuum model, k_a, k_d are not constants but are treated as functions of shear rate and physical properties of particles.

Table 2 Physical parameters used in the simulation

Symbol	**Value**	**Definition**
c_0	1000[mol/m^3]	Initial concentration
k_a	1x10^{-6} [m^3/(mol*s)]	Adhesion rate constant
k_d	1x10^{-3} -1x10^{-6}[1/s]	Detachment rate constant
θ_0	1000[mol/m^2]	Active site concentration
D_s	1x10^{-11}[m^2/s]	Surface diffusivity
D	1x10^{-9}[m^2/s]	Particle diffusivity in the fluid
k_B	1.38x10^{-23} [m^{2}kg s^{-2} K^{-1}]	Boltzmann constant
T	300[K]	Absolute Temperature
U	0-25[dyne/cm^2]	Maximum shear rate
λ	1x10^{-10}[m]	Equilibrium bond length

To initiate adhesion, nanoparticles must stay very close to the wall, inside the so called depletion layer, which is a near-wall layer that adhesion might happen. The thickness of the depletion layer is largely influenced by the flow rate, as demonstrated in figure 3. When drug

particles bind with receptor coated surface, drug concentration drops near the surface, effectively forms a “depletion layer” near the wall. Figure 3 shows the depletion layer at shear rates 0.1 mm/s and 1 mm/s respectively. As the flow rate increases the depletion layer thickness decreases due to greater particle flux and shorter retention time of the particles. The physical parameters used in the simulation are tabulated in Table 2. Similar model was developed by Haun and Hammer [23]to quantify the nanoparticle adhesion dynamics. But in this thesis work, the effect of shear rate and particle size on the binding dynamics of nanoparticles is studied.

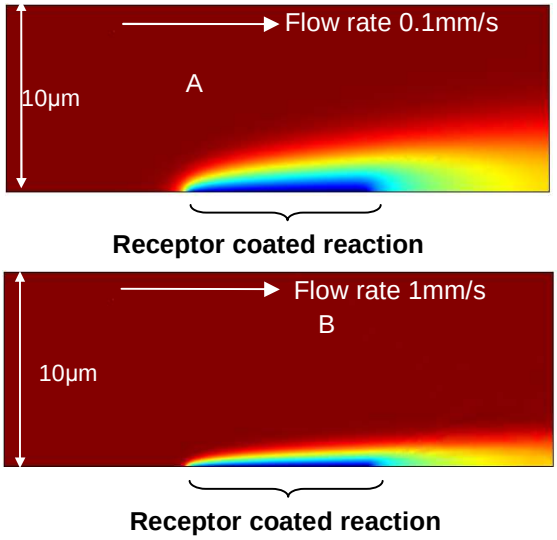

Figure 3 Depletion layer at shear rate of 0.1 and 1 mm/s. Particle concentration drops close to the receptor coated surface due to adhesion, forming a depletion layer. Colors: red = highest concentration; blue = lowest.

2.4. Nanoparticle adhesion probability model

The adhesion of nanoparticles on the target region is a chemical reaction process that is influenced by numerous factors. The adhesive strength of the particles is mediated by selective adhesion of molecules expressed over the target surface (receptors) and their counter-molecules conjugated at the particle surface (ligands). The dislodging forces on the particles are influenced by physiological factors such as the wall shear stress and by the particle properties such as shape and size. The adhesive forces are also influenced by biological factors as the surface

density of the receptors on the cell membrane, the surface density of the ligands grafted on the particle surface, the ligand–receptor family involved in the specific adhesive interaction and its affinity at the surface. Also, there are numerous physical factors that impact nanoparticle interaction with the vascular wall surface under vascular flow condition, such as nanoparticle-wall distance, nanoparticle size, ligand density, shear rate etc. In this thesis work, the influences of nanoparticle size, ligand density, and shear rates on adhesion kinetics are studied.

A numerical model is developed based on the work by Decuzzi and Ferrari [38]to describe the cell targeting processes of nanoparticles under flow conditions. In our study we considered spherical particles under shear flow. Decuzzi and Ferrari proposed a formula for adhesion probability of nanoparticles on the active site from the probabilistic kinetic formulation of McQuarrie [38],

$$P_a = m_r m_l K_a^0 A_c \exp[-\frac{\lambda f}{k_B T}] \qquad (2.4.1)$$

where m_r is receptor density on the targeted surface, m_l is the ligand density, f is the force acting per unit ligand-receptor pair which is a function of ligand-receptor contact area, $k_B T$ is Boltzman thermal energy of the system, λ is characteristic length of ligand-receptor bond and K_a^0 is the affinity constant of ligand-receptor pair. When the particles bind onto the receptors, the particles experience hydrodynamic forces. This force f is expressed by the equation,

$$f = \frac{F_{dis}}{A_c} = \frac{F}{A_c} + \frac{2T}{(A_c r_0)} \qquad (2.4.2)$$

where F_{dis} is the dislodging force due fluid flow, A_c is the surface area of contact of the particle, r_0 is the critical radius of the particle, T is the torque and F is the drag force which are components of the dislodging force along the direction of the flow. It is evident from Eq 2.4.2 that the force is a function of surface area of contact and particle size. This is because initially there is large area available for bond formation but after certain size of the particle, dislodging force

becomes a primary factor and the particles are carried away in the fluid medium. Force and Torque are functions of the local fluid shear rate defined as:

$$F = 6\pi a l \mu S F^s \qquad (2.4.3)$$

And

$$T = 4\pi a^3 \mu S T^s \qquad (2.4.4)$$

where a is the characteristic size of the particle, μS is the shear stress at the wall, l is the distance between the center of the particle to the substrate wall and F^s and T^s are the coefficients of drag and to torque which are functions of the spherical particle radius r. The contact area of the particle A_c is surface area of the spheroid below a separation distance h_o from the wall surface. It can be approximated as following:

$$A_c \cong \pi r_o^2 = \pi a^2 \left[1 - \left(1 - \frac{h_o - \delta_{eq}}{a} \gamma \right)^2 \right] \qquad (2.4.5)$$

Where, a is the radius of the particle, δ_{eq} is the equilibrium separation distance between the particle and wall surface, and γ is aspect ratio of the particle. Hence particle size is a decisive factor in particle adhesion probability. Figure 4 illustrates the effect of shear rate on dissociation probability $(P_d = 1 - P_a)$ of nanoparticles. As shown in figure 4, when the particle size increases, the dissociation probability increases for spherical particles. This is due to the fact that with increase in particle size, larger surface area is available for the bond formation, but after certain size of the particle, dislodging force becomes a dominant factor and it further reduces the probability of adhesion.

$$P_d = (1 - P_a)$$

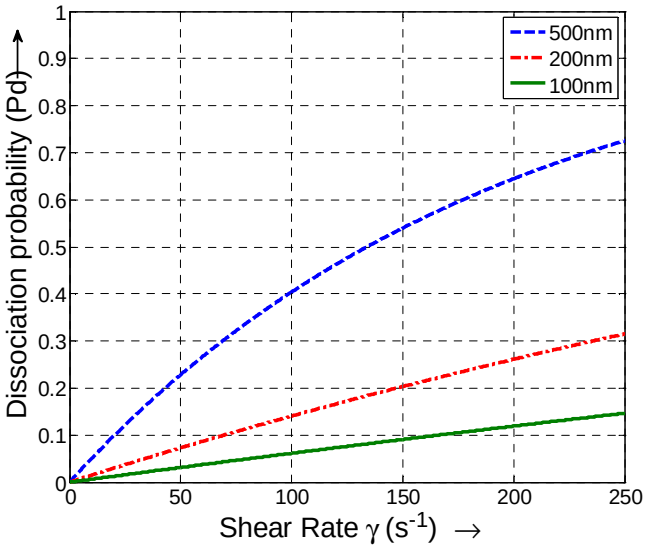

Figure 4 Dissociation probability vs. Shear rate on the reaction surface for nanospheres of different sizes.

Table 3 Physiological shear rate ranges in human body[43] [44] [45]

Vessel	**Shear Rate (s^{-1})**
Aorta	8
Artery	12.5
Arteriole	250
Capillary	10
Venules	25
Vein	10
Vena cava	3.3

2.5 Coupled particulate-continuum model

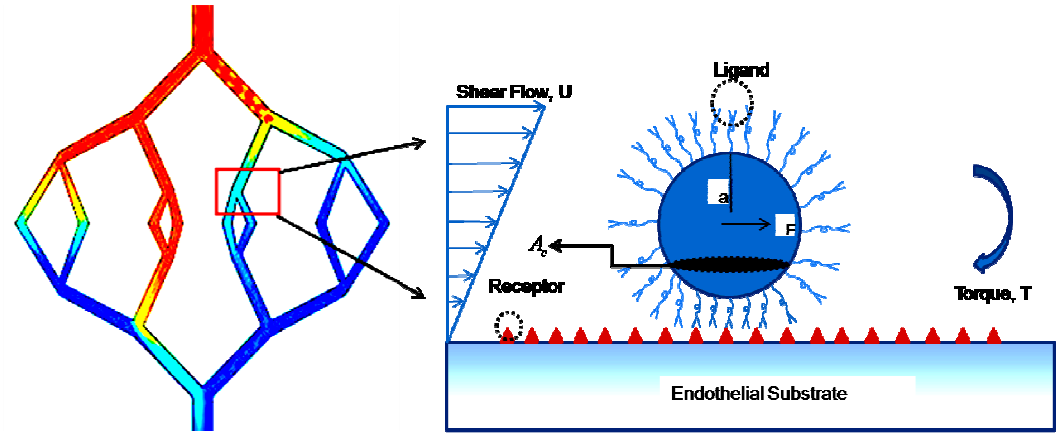

Figure 5 Multiscale model of targeted drug delivery

A coupled particulate-continuum model is developed to study the binding dynamics of nanoparticle targeting as illustrated in figure 5. The behavior of a material at the nanoscale is different from the same at the continuum level. It is crucial to understand the behavior of particles at different stages to design a drug delivery system. In our CFD simulation, the detachment rate which is a function of the particle size is calculated from the particulate theory of Decuzzi and Ferrari and is directly coupled with continuum model. The model involves a small parallel plate reactor with an active surface as the target region. The adsorption of particles between the reacting surface and the surrounding volume is coupled with transportation of particles by convection and diffusion. The developed model is used to study the effect of particle size, binding rates and shear rate on binding dynamics of nanoparticles on the target region.

2.6 Simulation results on nanoparticle adhesion dynamics

Continuum models[46] [23] have been used in the past to understand drug delivery mechanism. The advantage of continuum models is that they can effectively handle a large vascular network without much computational burden and providing quantitative analysis of the drug delivery process. However, it is unable to explore the adhesion process of individual

nanoparticles. Such a computational tool will help in understanding the adhesion dynamics of nanoparticles under varying vascular conditions with particle size considered.

2.6.1. Dynamic process of nanoparticle binding

Receptor density greatly influences the nanoparticle binding dynamics. Mechanical strength of adhesion is related to chemical affinity of receptor-ligand bonds. To investigate the effect of receptor density on nanoparticle binding dynamics, the deposition process of 500nm nanospheres is studied under physical flow condition of $1000s^{-1}$.

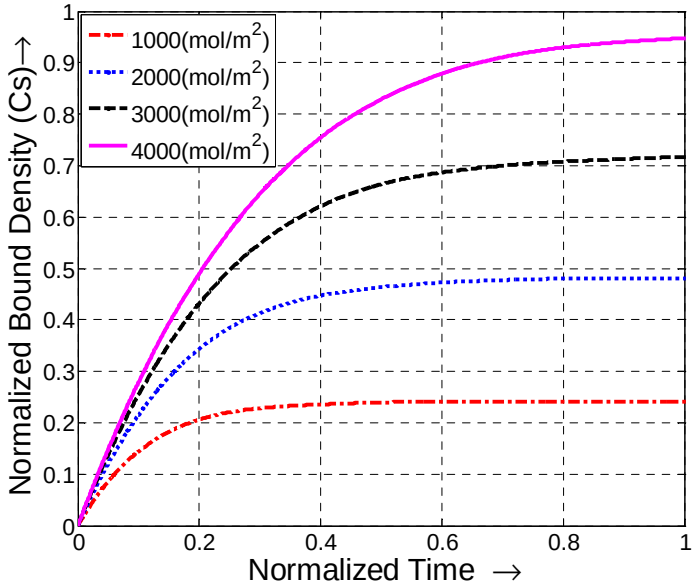

Figure 6 Normalized bound density vs. time for different receptor densities on the reaction surface.

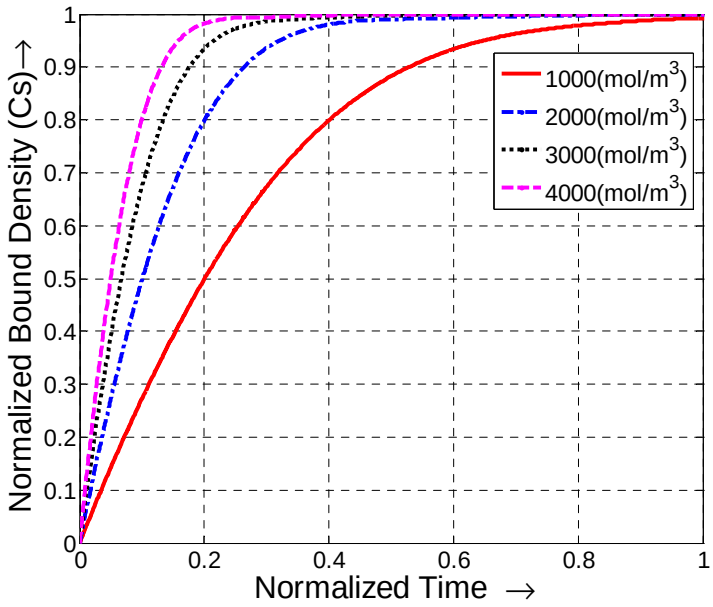

Figure 7 Normalized bound density vs. time for different initial concentration of particles.

The effect of receptor density[47] [48] is known to affect binding rates and hence the bound density of nanoparticles on the active site. The attachment rate increases with receptor density because there are more available sites for binding. The detachment rate decreases with increasing receptor density because a ligand that dissociates from one receptor has a finite probability of binding to another before escaping from the vicinity of the cell. The significance of ligand density is that the larger the density, stronger/faster the bond formation is. Therefore, large numbers of bond sites ensure firm adhesion of nanoparticles. Figure 6 demonstrates the effect of receptor density on the bound density of nanoparticles. Receptor density is increased from 1000 mol/m^2 to 4000 mol/m^2 under shear rate of 1000s^{-1}. It can be observed from figure 6 that bound density increases linearly with increasing receptor density. Here it is assumed that particle supply is larger than the available active sites. Figure 7 illustrates the effect of initial concentration of particles on bound density of particles. The receptor density is kept constant at 1000 mol/m^2 while the initial concentration of particles is varied. Simulation results show faster binding at higher

concentration of particles and also steady state is reached faster. This is because more particles are available for binding at higher concentration, increasing the attachment rate of particles and facilitating faster bond formation. The same steady state bound density is reached when all the receptors are occupied by the particles for binding.

Another important factor that affects the bound density of nanoparticles is the detachment rate since the particles are constantly exposed to shear stresses under vascular circulation. Additionally, collision of nanoparticles with RBCs and with the capillary walls may also detach particles from surfaces. The detachment rate affects the retention time of the nanoparticle thus determining the sustained drug release. The bound density of nanoparticles decreases with increase in the detachment rate as illustrated in figure 8.

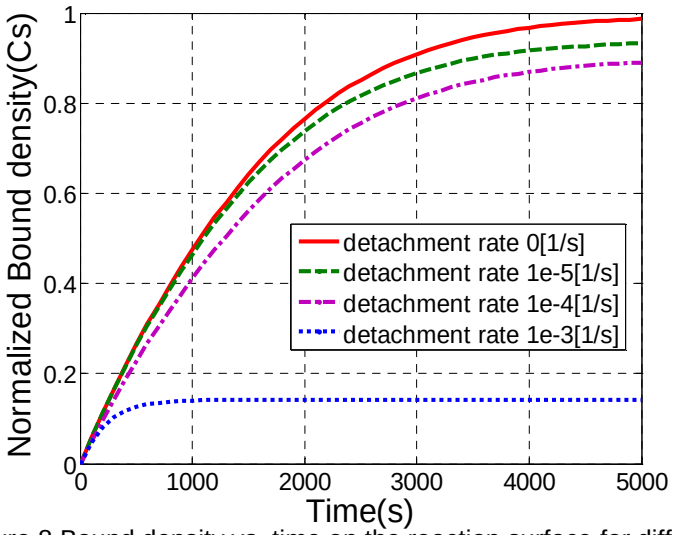

Figure 8 Bound density vs. time on the reaction surface for different detachment rates

2.6.2. Influence of shear rate and particle size on bound density with experimental validation

Farokhzad et al [49]have conducted experiments to study the effect of shear rate on nanoparticle binding dynamics. They observed that at low shear rates (1.1 dyne/cm^2) the average number of attached nanoparticle-aptamer bioconjugate was more than 10 per cell. However at a higher shear rate (4.5 dyne/cm^2), there was a significant decrease in attachment of

the particles. The adhesive force between the nanoparticles and the target surface is the result of specific biochemical forces due to receptor-ligand bonds. The kinetics of particle-surface interaction depends on the external hydrodynamics forces due to shear. Therefore, the targeting potential of a delivery carrier cannot be fully realized unless the binding performance is characterized under hydrodynamic flow conditions similar to the vascular circulation. The influence of shear stress in interstitial transport of nanoparticles in blood vessels has been an interest of research for scientists. The shear rate varies in the vascular system due to narrow vascular size and interstitial fluid pressure along the flow. The bound density of nanoparticles under different shear rates is studied for particles of different sizes. The bound density of nanoparticles under different shear rates is illustrated in figure 9. The simulation results elucidates that increase in shear rates reduces bound density of nanoparticles and the bound density also varies with the size of nanoparticles. Results imply that binding probability rapidly drops for nanospheres with increase in shear rate. The bound density of nanoparticles decreases with particle size since larger particles are under higher shear. The continuum results of bound density vs. shear rate were validated with the experimental results. We can see from the plot that the results from the continuum model are in good agreement with the experimental results (process described later in the section). The size of the nanoparticles greatly influences the drag force and the surface area of the particles. As the particle size increases, the fluid drag forces acting on the particle also increases and hence the dislodging forces acting on the larger particle is much greater than that acting on the smaller particle. Figure 10 demonstrates the effect of bound density at two different shear rates. Particles are supplied for a limited period of 30 seconds. The dashed line indicates the start of detachment period where the particle supply is cut off and washed by buffer solution. We can observe faster binding at higher shear rate and also faster detachment. Our model demonstrates that shear stress on the particle due to fluid flow can have significant effect on the binding characteristics of targeted drug delivery vehicles. The results from our continuum model provide a direct correlation between bounded particle densities

and nanoparticle properties, thus establishing criteria necessary to predict adhesion dynamics within the context of specific targeting applications.

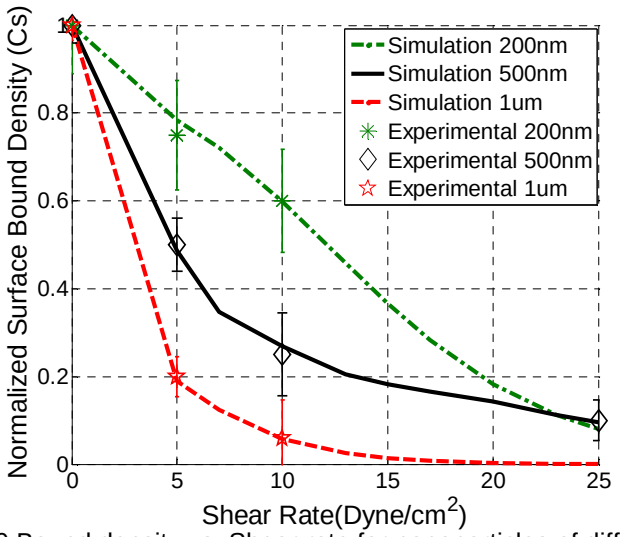

Figure 9 Bound density vs. Shear rate for nanoparticles of different sizes.

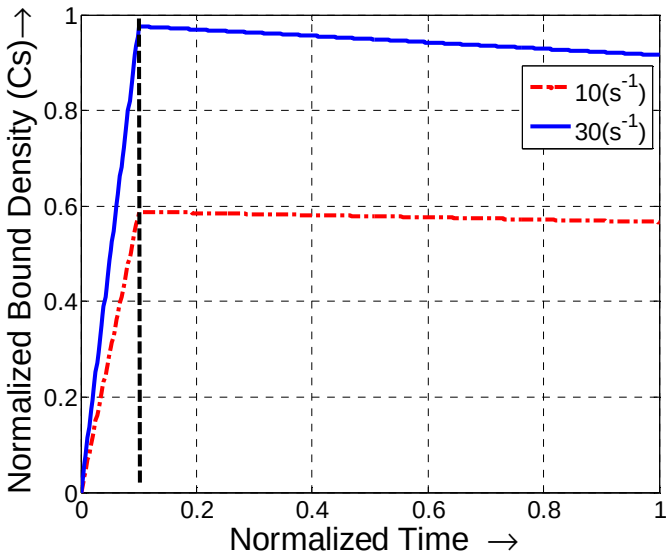

Figure 10 Bound density vs. time at different shear rates

Experiments were carried out on GPIb conjugated PLGA (Poly Glycolic Acid Polymer) nanoparticles. The nanoparticles were formulated using standard double emulsion method and

characterized using fluorescence microscope. The particle adhesion on vWF (Von Willebrand factor – a blood glycoprotein) coated surfaces under different shear rates were studied using different size nanoparticle samples. vWF culture dishes were assembled in the circular flow chamber system shown in figure 11. Nanoparticles in suspension were flown over the surface at various shear rates (0-25 dyne/cm^2). The flow chamber has 3 ports connected to inlet, outlet and vacuum pump respectively. The vacuum provides an air tight seal so that only the coated area exposed to the flow acts as the receptor. To investigate the effects of shear stress on binding of nanoparticles, the vWF coated culture dishes were assembled in circular flow chamber. GPIb nanoparticles in suspension were flown over the vWF coated surface at different shear rates for 30 minutes. After the flow experiments, the amount of nanoparticles bound to the 35mm culture dishes were quantified using fluorescence measurements. Figure 12 shows the schematic of circular flow chamber and the gasket dimensions. The shaded region on the gasket image is the actual receptor coated area available for binding.

Figure11 Circular Flow Chamber.

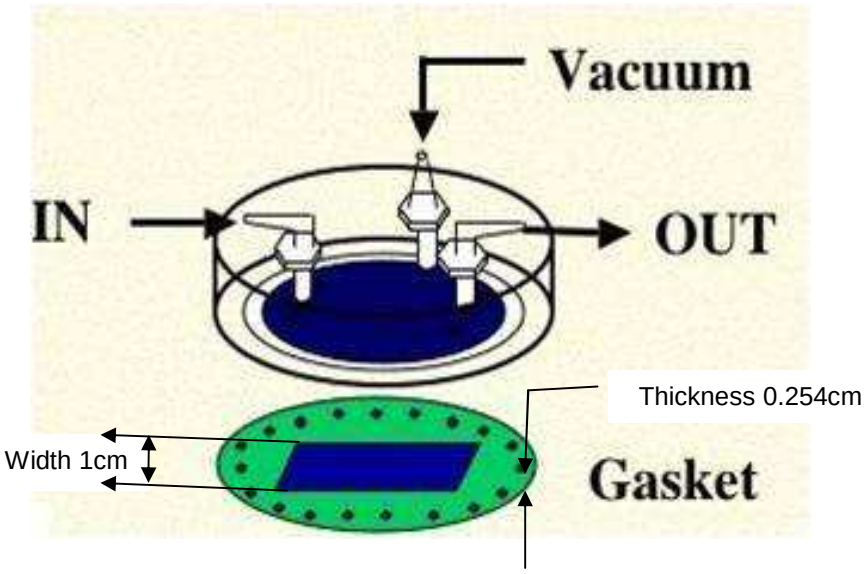

Figure12 Schematic of Circular Flow Chamber

2.7. Nanoparticle deposition and distribution in blood vessel network

Another application of developed model is to determine nanoparticle deposition and distribution in vascular geometry. To demonstrate capability of the developed model in this thesis work, a case similar to real targeted drug delivery in blood vessel is developed and executed. When a portion of the blood vessel is injured, a significant P-selectin is expressed on damaged endothelial cells [50], which can be targeted by nanoparticles coated with GPIb ligand. In this model the convection diffusion in the 2D fluid domain is coupled with the adhesion reaction occurring only on the reaction surface which mimics the target site for drug delivery. Figure 13 shows drug concentration gradient in the vascular network. Nanoparticle drug carriers of a given concentration are injected at the top inlet and are transported through the network along with fluid flow. The left branch of the network is assumed to a receptor coated target surface that can form bonds with ligands on drug nanoparticle surface. The particle depletion layer is clearly shown in

the target region. The density of deposited drug particles on the wall surface is plotted in figure 14, which indicates that most drug particles are deposited at the entrance of the target region, while the rest of the target region has low density of deposited drug particles. There are no particles deposited in the healthy branch assuming the ideal situation of zero non-specific adhesion. The results of targeted drug delivery are illustrated in figure 13. It is evident from the figure that there is adsorption of the drug on the blood vessel as shown in figure 14. In the region where the vessel is modeled as non active region most of the drug is diffused through. Such non-uniform distribution pattern indicates possible impaired delivery dosage within the target region, which is important for delivery efficacy prediction and dosage planning.

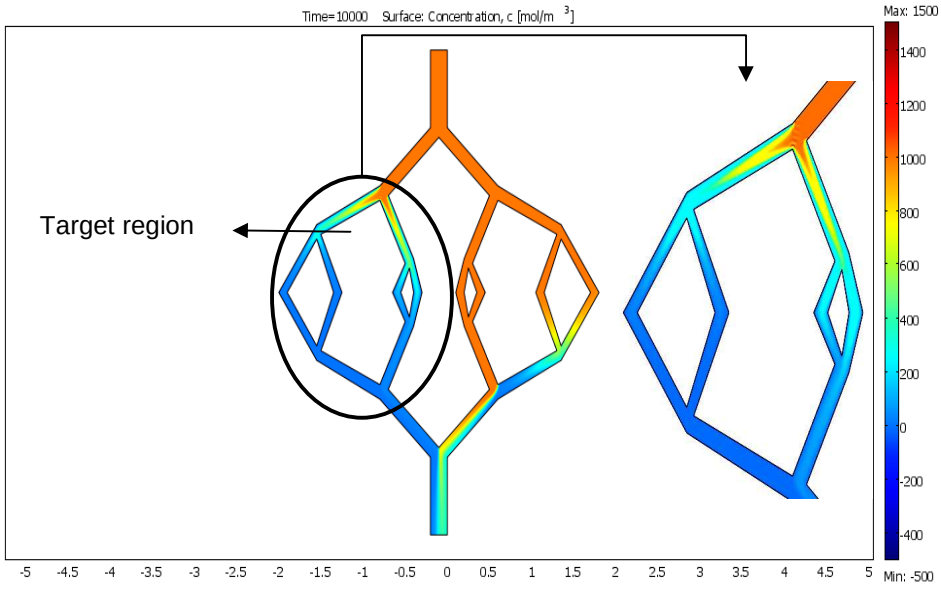

Figure 13 Drug concentration as it flows from parent vessel through the vascular network with the receptor coated target region marked by the black-circle. Colors: red = highest concentration; blue = lowest

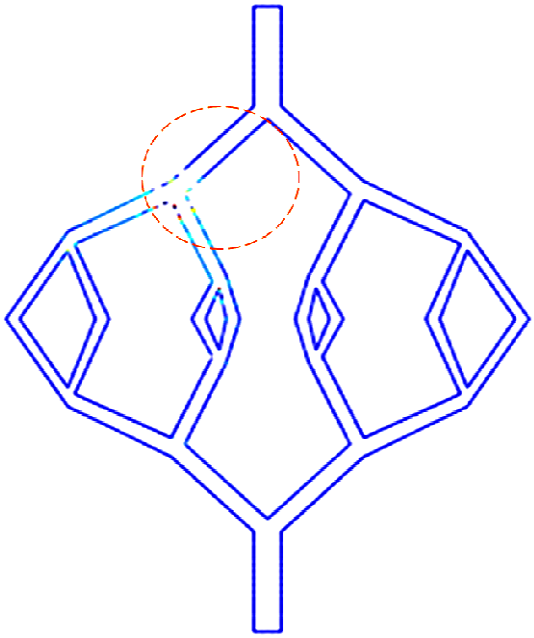

Figure14 Density of bounded drug particle on the wall surface.

Table 4 Physical parameters used in blood vessel network simulation

Symbol	Value	Definition
c_0	1000[mol/m^3]	Initial concentration
k_a	1x10^{-6} [m^3/(mol*s)]	adhesion rate constant
k_d	1x10^{-9}[1/s]	detachment rate constant
θ_0	1000[mol/m^2]	Active site concentration
D_s	1x10^{-11}[m^2/s]	Surface diffusivity
D	1x10^{-6}[m^2/s]	Particle diffusivity in the fluid
V	1[mm/s]	Maximum velocity
ρ	1063[kg/m^3]	Blood density
η	0.003[Pa.s]	Blood dynamics viscosity

In this chapter, a continuum model is developed to study the nanoparticle adhesion dynamics. This model effectively describes the targeted drug delivery process. Using this developed numerical model, the influence of nanoparticle size, receptor density, and flow conditions on nanoparticle adhesion dynamics is explored. This computational model can be used to characterize multiple parameters simultaneously and therefore optimize the physical properties of therapeutic and diagnostic particles prior to their *in vivo* evaluation.

CHAPTER 3

MODELING DIEP FLAP PERFUSION

3.1. Introduction to breast reconstruction and DIEP flap

Every year more than 250,000 women[51] in America alone face breast cancer which is second only to lung cancer as the leading cause of cancer accounting for about 27% of all kinds of cancers. Women with breast cancer choose surgery that removes only a part of the breast tissue or the entire breast which is called mastectomy. The surgery includes the reformation of a natural looking areola and nipple so that the breast is about same size as it was before. The breast reconstruction surgery is not only essential but has been mandated by federal law in the United States since 1998[51]. Several types of operations can be done to reconstruct the breast. Either a breast implant or a tissue of the own patient or a combination of two can be used to reconstruct the breast[52].

- Implant procedures: The most common implant is a Saline filled implant. It is a silicone filled with salt water. They are not used as much as they were in the past due to concerns that silicone leakage might cause immune system diseases.
- Tissue Flap procedures: These procedures use tissue from the patient tummy, back, thighs or lower back to rebuild the breast. There are several types of flap procedures depending on the tissue used for the reconstruction of the breast.

- TRAM (transverse rectus abdominal muscle) flap: The TRAM flap procedure uses tissue and muscle from the tummy (the lower abdominal wall). The tissue from this area alone is often enough to shape the breast, and an implant may not be needed. The skin, fat, blood vessels, and at least one abdominal muscle are moved from the belly (abdomen) to the chest. There are two types of TRAM flaps.

- Pedicle Flap: Pedicle flap leaves the flap attached to its original supply and tunnels it under the skin to the breast area.
- Free Flap: In a free flap the tissue including the skin, fat, blood vessels and muscle for the implant is cut off free from its original location and then attached to the blood vessels in the chest under microscope.
- DIEP (Deep Inferior Epigastric artery Perforator) flap: The DIEP flap uses fat and skin from the same area as in the TRAM flap but does not use the muscle to form the breast mound. This results in less skin and fat in the lower abdomen. This method uses a free flap, meaning that the tissue is completely cut free from the tummy and then moved to the chest area. This requires the use of a microscope to connect the tiny vessels.
- Gluteal Free Flap: The gluteal free flap or SGAP (superior gluteal artery perforator flap is newer type of surgery that uses tissue from the lower back, including the gluteal muscle, to create the breast shape. It is an option for women who cannot or do not wish to use the tummy sites due to thinness, incisions, failed tummy flap, or other reasons. The method is much like the free TRAM flap mentioned above. The skin, fat, blood vessels, and muscle are cut out of the lower back and then moved to the chest area under microscope.

DIEP is a tissue flap procedure that uses fat and skin from the abdomen to create a new breast mound after a mastectomy. Perforator flaps have allowed the transfer of the patient's own skin and fat in a reliable manner with minimal donor site morbidity[53]. Most women who have had or will have mastectomies for breast cancer are possible candidates for a DIEP flap. In addition, this flap may be used for women requiring additional breast tissue for reconstruction of defects such as a congenital breast deficiency, a lumpectomy defect or for autologous breast augmentation[54]. Most women have enough extra tissue in their abdomen making it the most common donor area to create a new breast mound. Some of the advantages of DIEP are, no muscle is moved, less pain and faster recovery than a TRAM flap. A DIEP flap, however also

includes the movement of an artery and vein from the tissue flap to the chest so that the transplanted tissue can be supplied with blood. During this procedure an incision is made along the abdomen to remove a layer of skin and fat with arteries and veins. They bring a dependable blood supply in the flap. Allen and Treece[55] successfully performed the first DIEP flap for breast reconstruction by transferring the abdominal skin and fat from the same donor area of a TRAM flap while sparing the underlying rectus abdominus muscle. This provided essentially the same soft tissue for reconstruction while significantly reducing the morbidity to the abdominal wall, thereby minimizing donor site morbidity and pain while shortening recovery time[56] [57] [58]. In surgeons experience, the DIEP flap has shown to be a safe, consistent and reliable flap for breast reconstruction[59]. The DIEP flap is based on deep inferior epigastric artery and vein. Two rows of perforating arteries and veins penetrate the rectus muscle on each side of the abdomen to provide the blood supply for the overlying skin and fat. The perforating vessels, which supply the overlying skin and fat are carefully followed through the rectus muscle to their origins from the deep inferior epigastric vessels. The rectus muscle itself is spared and traumatically spread apart in the direction of the muscle fibers during dissection. Figure 15 illustrates typical markings of a DIEP flap in the lower abdomen region before dissection.

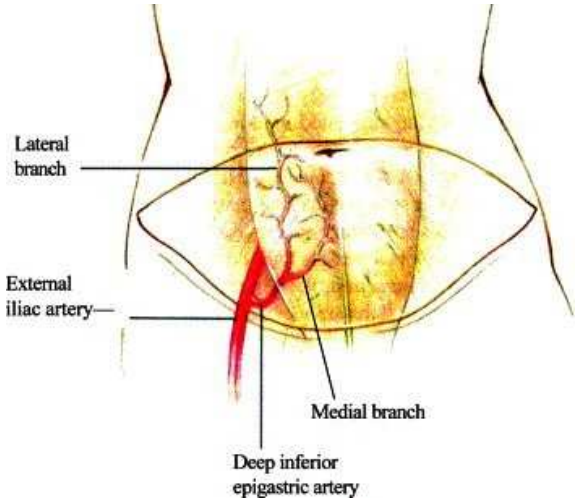

Figure 15 Typical preoperative marking on the lower abdomen of a patient undergoing breast reconstruction using the DIEP free flap [2].

The internal mammary or thoracodorsal vessels are used as recipient vessels. If a large lateral perforator is found, the flap may be based on this vessel. Additional perforators in the same row in series or in parallel may also be dissected and included with the flap for additional perfusion. If no large lateral row perforators are found, the medial row is approached for connection. If no dominant single perforators are found, two or more smaller perforators in the same lateral or medial row may be taken to perfuse the flap [2]. In cases where more than one large perforator is present, the perforator with a more central location to the proposed flap is utilized. According to surgeons experience, approximately 25% of flaps are based on one perforator, 50% on two perforators and 25% on three or more perforators[60]. Hence the number of perforators and the fashion in which they are connected is a critical factor in determining the perfusion performance of the flap. The aim of this thesis work is to develop a mathematical model to determine the optimal position, number and the type of connection for perfusion of the flap. Figure 16 shows a DIEP flap with a deep inferior epigastric artery and perforators.

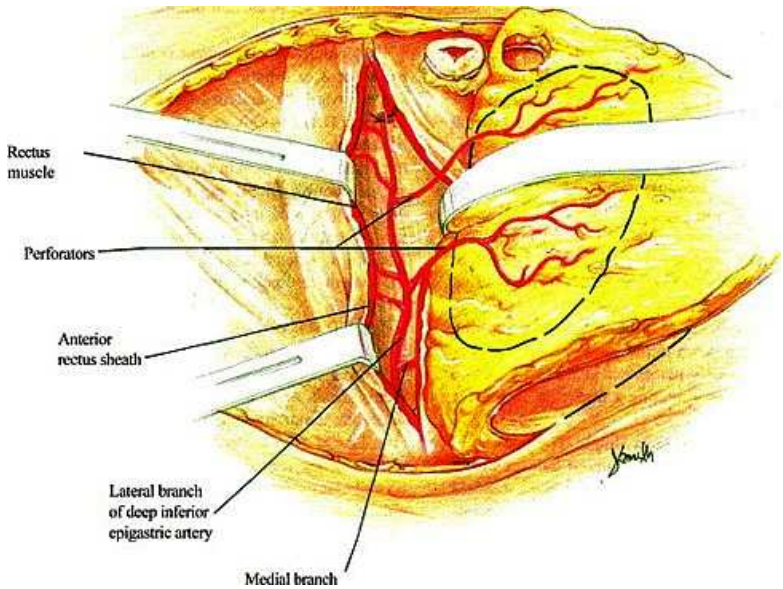

Figure 16 Perforator vessels of the lateral branch of the deep inferior epigastric artery visible running through the rectus sheath [2-3].

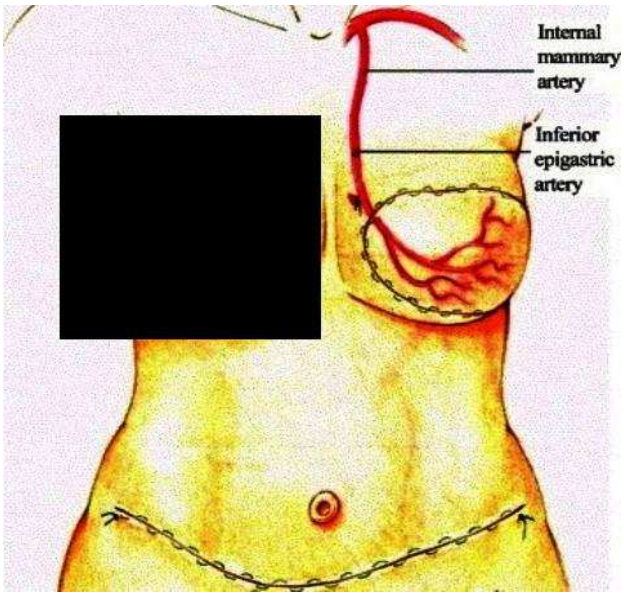

Figure17 Recipient and flap arteries after anastomosis and flap inset [2].

As discussed earlier, it is important to determine how the size and number of perforators affect the perfusion of the flap to minimize patient morbidity. However it has not been established how the vascularity is affected when a single perforator is used and all other perforators are ligated as in case of pedicle perforator flaps. In pedicle perforator flaps all the perforators except one are ligated in order to transfer the flap and rotate it by 180 degree. Patel and Keller [36] developed a mathematical model[61] [62] to study the effect of number and size of perforators on the vascularity of the flap. They compared the system of perforators to a circuit with multiple resistances in parallel and concluded that the best perfused flap involves use of the largest diameter vessel. Inclusions of other smaller perforators in addition to the largest diameter perforator will reduce the overall resistance, but this reduction in resistance is dependent on the diameter of the additional perforator. However, Patel and Keller's paper did not address the interconnectivity of the capillary network within the flap and also flow though a single perforator.

In this thesis work, a continuum model and also a reduced model similar to Patel and Keller's model are developed accounting for interconnections in the flap.

3.2. Continuum model of DIEP flap perfusion

A continuum CFD model is developed to analyze the effect of size, number and interconnectivity of perforators on the perfusion of the vascular network of the flap. Finite element method is employed to solve the Navier-Stokes equations for the fluid flow in the vascular network. The incompressible Newtonian fluid is governed by Navier-Stokes equation, $-\nabla p+\mu\left(\nabla^2 \mathrm{v}\right)+\rho \mathrm{b}=\rho \dot{\mathrm{v}}$, where ρ and μ are density and dynamic viscosity of the blood respectively. We measured the average velocity of the flow near the exit of the perforators which gives a measure of resistance of the network. Vessel resistance(R) is directly proportional to length(L) of the vessel and dynamic viscosity(μ) of the blood and inversely proportional to the fourth power of the radius(r^4) of the vessel[63].

$$R=\frac{8\eta L}{\pi r^4} \tag{3.2.1}$$

The relation between the blood flow *Q*, pressure and resistance in the vessel is defined by Poisseuille's equation, where ΔP is the pressure difference across blood vessel length *L.*

$$Q=\frac{\Delta \mathrm{P}*\pi*r^4}{8*\mu*L}=\frac{\Delta P}{R} \tag{3.2.2}$$

It can be observed from Eq 3.2.1 that the vessel resistance is directly proportional to the length of the vessel and the viscosity of the blood, and inversely proportional to fourth power of the radius. Therefore a small change in the radius increases the resistance in the vessel considerably. A small change in radius will lead to large change in the resistance. While the length of the vessels and the blood viscosity is fairly constant in the human anatomy [63], there are significant changes in the radius of the blood vessel throughout the network due to contraction and relaxation of the

muscles and also branching of the blood vessel network. Therefore the vessel radius has dominant influence on the flow.

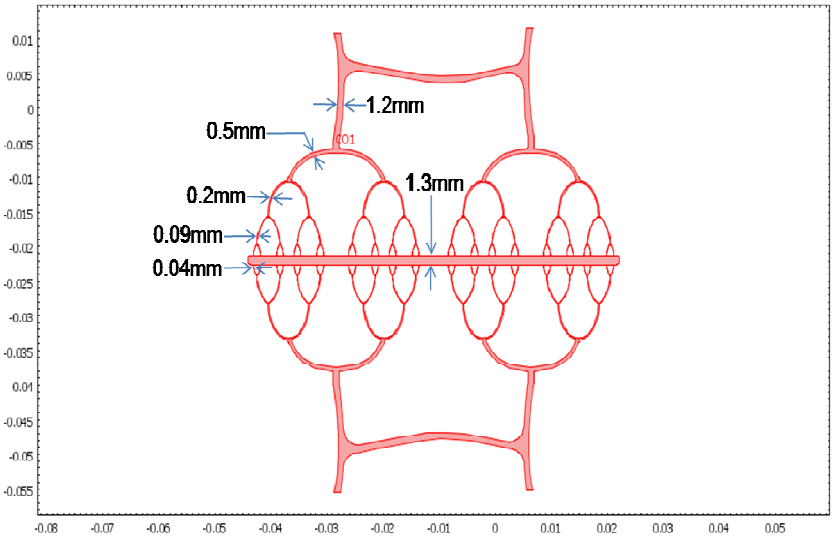

Figure 18 Dimensions of the vessel network

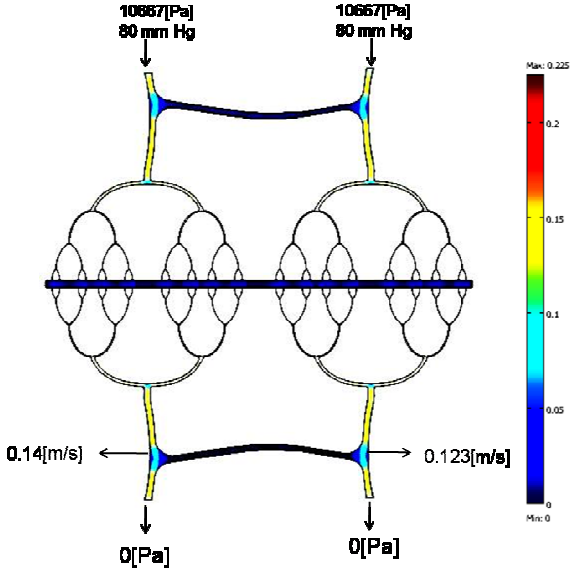

Figure 19 Velocity profile of the network and boundary conditions at the inlet and outlet of the perforators.

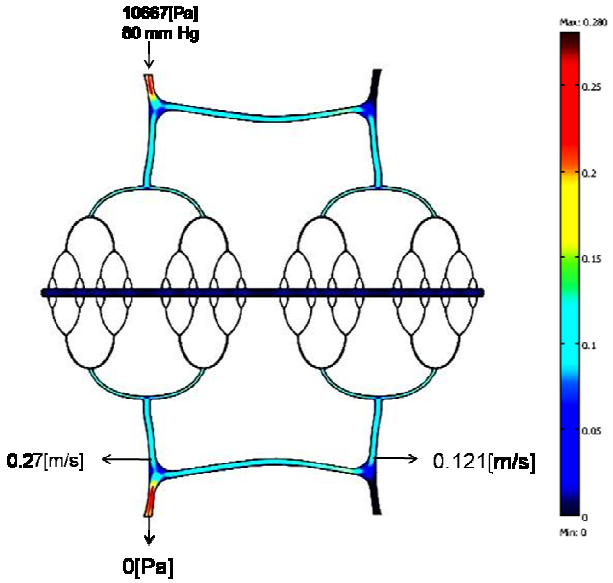

Figure 20 Velocity profile of the network and boundary conditions with right perforator ligated.

Vascular network is usually constructed by binary trees method [64]. The binary trees represent vascular trees which are set of nodes characterized by their spatial position, blood rate and pressure[64]. Jurczuk et al [64] have developed vascular network accounting for successive bifurcations of the vessels and perfusion process. A blood vessel network is developed with successive reduction in size along the branch of the network as shown in figure 18. The normal blood pressure range in the humans is in the range 70 mm Hg to 130 mm Hg [65]. A diastolic (lower number) pressure of 80 mm Hg which is equivalent to 10667 Pa is used in our simulation to study blood perfusion in the vascular network. The blood density at 37^0C is 1060 [kg/m^3] [66] and dynamics viscosity is 0.003 [Pa.s] [67] are used in our CFD simulations. The velocities are recorded before and after ligating the right perforator and are compared in figure 19 and figure 20. The velocity nearly doubled towards the exit after ligating the right perforator. The blood velocity is indicated by color in figure 19 and figure 20 respectively. The outlet blood velocity for

two perforators is 0.14 m/s while the velocity for a single perforator is 0.27 m/s. After ligating the right perforator, though there is an increased velocity in the left perforator, the velocity in the right perforator remained unchanged. It was also observed that even though the dimension of the left perforator was kept intact after ligating the right perforator, perfusion in the network was unchanged for the same inlet pressure conditions. These results agree with the observations made by the surgeons that a single large perforator gives better vascularity [60].

3.3. Reduced models of vascular system

CFD simulations are usually restricted to small size domains due to computational memory and large degrees of freedom. Computational complexity may be reduced by adopting reduced models in which the 3D flow models are reduced to 1D model. One dimensional modeling of vascular network was first introduced by Euler et al [68]. They developed partial differential expressions to represent the arterial network based on conservation of mass and momentum of fluid flow in the vascular network. 1D models [69] [70] [71]and Windkessel (German word for air chamber) models [72] [73] have been widely employed to study blood flow in arterial network. Windkessel models are used to study hemodynamic variables in blood vessels. Analysis of arterial network is described by parameters such as arterial compliance, peripheral resistance and pressure difference across the vessel. Characteristics of the arterial system can be determined by analyzing Windkessel models. Alastruey et al[71] and Westerhof [72] have successfully employed Windkessel models to study pulse wave propagation in cerebral circulation and arterial heart and valve studies, resistance in the arterial system respectively. Kumar et al[74] developed a finite element model of human vascular network consisting of 55 arteries and successfully predicted the influence of velocity and pressure in the arterial network. A similar Windkessel model is developed to support the continuum model results of perfusion of DIEP flap. Interconnections in the vascular network are also considered in the mathematical model.

3.4. Mathematical model based on current-resistance circuit analogy

We developed a theoretical model based on the circuit analogy theory. Figure 21 shows CT image of a DIEP flap. As we see from the image the flap is a random network of blood vessels with interconnecting vessels. Perfusion in the network is studied with a mathematical model accounting for interconnectivity. We compared the perforators to a circuit with multiple resistances in parallel. The volume rate in the network is defined by the equation $Q = \frac{\Delta P}{R}$ (3.2.2) for a circular cross section vessel. It can be compared to electrical circuit as $I = \frac{V}{R}$ where *R* is the equivalent resistance, *I* is the current in the circuit and *V* is the potential difference across the network. Blood flow is treated analogous to current, and resistance is treated analogous to $8\eta L/\pi r^4$ (3.2.1).

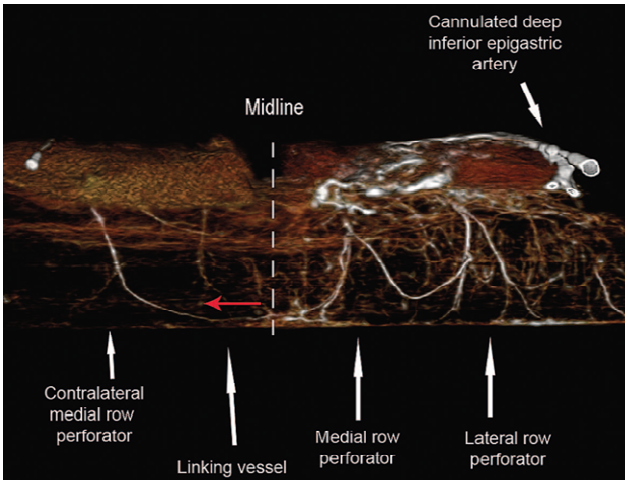

Figure 21 Interconnectivity of perforator flap [1]

First, we considered a model of flap vascular network without linking vessels. Let's assume that there are two equivalent perforators in this circuit system, as in figure 22. We assumed an Ohm's model, in which R_P is the resistance of perforator, R_S is the resistance of small vessel, R_L is the

resistance of linking vessel , R_C is the resistance of capillary systems and *P* is the voltage across the circuit.

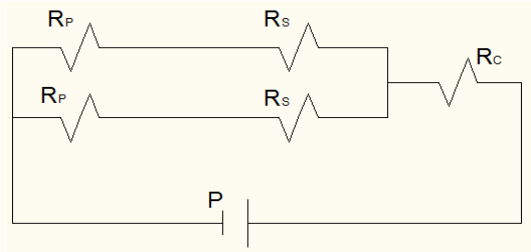

Figure 22 Two parallel perforators in series without linking vessel

The total resistance in a circuit with two parallel perforators in series in a vessel network without linking vessel is

$$R^{2\,perforator}_{without\ linking\ vessel} = R_C + \frac{1}{\frac{1}{R_P+R_S}+\frac{1}{R_P+R_S}} = R_C + \frac{R_P}{2} + \frac{R_S}{2} \tag{3.4.1}$$

The total current in a circuit with two parallel perforators in a vessel network is

$$I^{2\,perforator}_{without\ linking\ vessel} = \frac{P}{R_C + \frac{R_P}{2} + \frac{R_S}{2}} \tag{3.4.2}$$

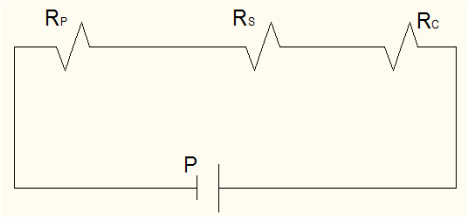

Figure 23 Vessel network with one of the perforator ligated without linking vessel

If we ligate one perforator in the circuit system as in figure 23, the total resistance in circuit is

$$R^{1\,perforator}_{without\ linking\ vessel} = R_C + R_P + R_S \tag{3.4.3}$$

The total current in circuit after ligating a perforator is

$$I_{\substack{1\,perforator\\ without\ linking\ vessel}} = \frac{P}{R_C + R_P + R_S} \tag{3.4.4}$$

Comparing (3.4.2) and (3.4.4), if we don't have linking vessel, adding a 2nd perforator significantly decreases network resistance and increases current in the network. Second, we considered a model with linking vessels. We assume two equivalent perforators in the circuit system as figure 24. Due to the symmetry in the system, there would be no flow in the linking vessel. So we do not need to consider the resistance of linking vessel in this case.

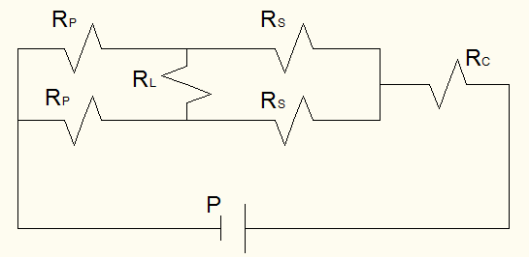

Figure 24 Two parallel perforators connected by a linking vessel in series with capillary network

The total resistance of the circuit with two perforators and a linking vessel is:

$$R_{\substack{2\,perforator\\ with\ linking\ vessel}} = R_C + \frac{1}{\frac{2}{R_P} + \frac{1}{R_L} + \frac{2}{R_S}} \tag{3.4.5}$$

The total current in circuit with two perforators and a capillary with a linking vessel is:

$$I_{\substack{2\,perforator\\ with\ linking\ vessel}} = \frac{P}{R_C + \frac{1}{\frac{2}{R_P} + \frac{1}{R_L} + \frac{2}{R_S}}} \tag{3.4.6}$$

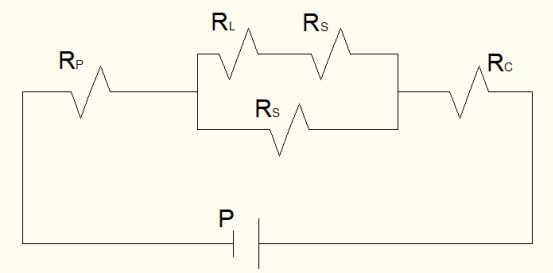

Figure 25 Perforator in series with capillary, when one of the perforator is ligated

If we ligate one perforator in the circuit system above, as shown in figure 25, total resistance in circuit is:

$$R^{1\,perforator}_{with\ linking\ vessel} = R_P + R_C + \frac{1}{\frac{1}{R_S} + \frac{1}{R_S + R_L}} = R_P + R_C + \frac{R_S^2 + R_S R_L}{2R_S + R_L} \tag{3.4.7}$$

The total current in the circuit with linking vessel is:

$$I^{1\,perforator}_{with\ linking\ \text{vessel}} = \frac{P}{R_P + R_C + \frac{R_S^2 + R_S R_L}{2R_S + R_L}} \tag{3.4.8}$$

From the equations above, we found that

$$R^{1\,perforator}_{without\ linking\ vessel} > R^{2\,perforator}_{without\ linking\ vessel} \Rightarrow I^{1\,perforator}_{without\ linking\ vessel} < I^{2\,perforator}_{without\ linking\ vessel}$$

$$R^{1\,perforator}_{with\ linking\ vessel} > R^{2\,perforator}_{with\ linking\ vessel} \Rightarrow I^{1\,perforator}_{with\ linking\ vessel} < I^{2\,perforator}_{with\ linking\ vessel}$$

So it is evident that the resistance of 1-perforator model is always larger than that of 2-perforator model and the flow of one perforator model was smaller than that of 2-perforator model for cases with or without linking vessels. However, the difference in resistance/flow between single perforator and 2-perforator case is quite small when considering linking vessels. As estimation, we evaluate the following ratios:

$$\frac{I^{1\,perforator}_{without\ linking\ vessel}}{I^{2\,perforator}_{without\ linking\ vessel}} = 1 - \frac{R_P + R_S}{2\left(R_C + R_P + R_S\right)} \tag{3.4.9}$$

$$\frac{I^{1perforator}_{with\ linking\ vessel}}{I^{2perforator}_{with\ linking\ vessel}} = 1 - \frac{R_S^2}{(2R_S + R_L)(R_C + R_P + R_S)} \tag{3.4.10}$$

If we assume $R_C = R_S = R_L = R_P$, then

$$\frac{I^{1perforator}_{without\ linking\ vessel}}{I^{2perforator}_{without\ linking\ vessel}} = 66.7\% \tag{3.4.11}$$

$$\frac{I^{1perforator}_{with\ linking\ vessel}}{I^{2perforator}_{with\ linking\ vessel}} = 88.9\% \tag{3.4.12}$$

Comparing (3.4.11) and (3.4.12) it can be found that there is significant increase in the current through the network when the effect of interconnections is considered. For a more realistic estimate, we considered resistances of various blood vessels in human blood vessel network. The human vascular network consists of arteries and arterioles, veins and venules, capillaries and sinusoids. Table 5 shows the dimensions of the blood vessels in human vascular network.

Table 5 Blood vessel size in human vascular network[75] [76] [77]

Blood vessel	**Diameter**
Artery	0.1mm-10mm
Arterioles	20µm-30µm
Veins and venules	1mm-1.5cm
Capillaries	5µm-10µm
Sinusoids	30µm-40µm

The diameter of arterioles usually ranges from 20µm to 30µm at the end where they connect to capillaries. The capillaries have a diameter less than that of red blood cells typically about 5µm-7µm [27, 78] [75] in diameter. Now let's take a look at the actual resistance of various vessels in human system. There are about 40 billion capillaries and 400 million arteries[79] in human body[80]. Therefore we assumed an average of 100 capillaries connected to an artery, and an

artery branches into 2 arterioles. Since the resistance in the vessel is inversely proportional to fourth power of the radius, we have,

$$\frac{\text{Resistance}_{\text{one capillary}}}{\text{Resistance}_{\text{one artery}}}=\frac{(0.1\times10^{-3})^4}{(10\times10^{-6})^4}=10^4 \quad \text{and} \quad \frac{\text{Resistance}_{\text{one arteriole}}}{\text{Resistance}_{\text{one artery}}}=\frac{(0.1\times10^{-3})}{(3\times10^{-5})}=123.45 \qquad (3.4.13)$$

Also, assuming capillaries are connected in parallel, we have $R_{effective\ capillaries}=\frac{R_{one\ capillary}}{100}$ and

In Equation 3.4.11, if we assume $R_p=R_{artery}$ and $R_S=R_L=R_{arteriole}$ and $R_C=R_{effective\ capillaries}$ then

(3.4.11) can be restated as $$\frac{I^{1\ perforator}_{without\ linking\ vessel}}{I^{2\ perforator}_{without\ linking\ vessel}}=1-\frac{R_P+R_C}{2(R_C+R_P+R_S)}=61.45\% \qquad (3.4.14)$$

and (3.4.12) with linking vessel becomes $$\frac{I^{1\ perforator}_{with\ linking\ vessel}}{I^{2\ perforator}_{with\ linking\ vessel}}=89.52\% \qquad (3.4.15)$$

Thus, it can be concluded that if we don't have linking vessel, adding a second perforator significantly decreases the network resistance and increased current in the network. However, by considering the linking vessel effect, ligating a perforator would only decrease current by 10% compared to 40% without linking vessel. Thus ligating one perforator at the cost of traumatizing the tissue and operative cost is not suggested. This also supports the observations made by the surgeons that using a single large perforator gives better perfusion. A framework for choosing proper size of the flap and number of perforators for better perfusion is established in through this work.

CHAPTER 4

CONCLUSION AND FUTURE WORK

4.1 Nanoparticle adhesion dynamics

Continuum modeling of targeted drug delivery system provides quantitative prediction of the drug transportation in biological systems. It can be utilized to evaluate efficiency of drug delivery, and to estimate dose response and toxicity. To understand the underlying transportation and deposition mechanism, a novel multi-scale computational modeling tool has been developed. The uniqueness of the proposed method lies on the fact that the attachment and detachment rates are not treated as constants. Instead, they are directly linked to physical properties of particles (size and ligand density) and flow rate through the particulate model. Since the proper drug dosage choice relies on determination of the adhesion and detachment rates of the nanoparticles at the active region [81], it is essential to determine the adhesion and detachment rate constants in order to understand the mechanism of delivery. The adhesion and detachment dynamics largely depends on local flow and particle size. We postulate that our continuum models can be used to test multiple parameters simultaneously and therefore optimize the physical and chemical properties of therapeutic and diagnostic nanoparticles prior to their *in vivo* evaluation. We have also demonstrated the effect of shear rate on bound density of nanoparticles. Higher shear rates tend to accelerate the adhesion process since more number of particles flow over the receptor area during the same time and hence more number of particles available for binding at the same time. But also as the shear rate increases the bounded particle density decreases which is due to the increased detachment rate at higher shear rates. Under the same shear rate, bounded particle density is higher for smaller particles compared to larger particles. This is because larger particles experience larger dislodging force, thus the higher detachment rate. Thus we can determine the optimum shear rate and the size of the particles for

desired drug efficiency depending on the size of the blood vessel and the flow rate in the vessel. The influence of nanoparticles size and ligand density on nanoparticle adhesion dynamics has been studied qualitatively. Upon contact of the nanoparticles to the receptor area, the probability of adhesion is also determined by receptor density. Receptor density increases the probability of adhesion of nanoparticles. The result reveals that there is increase in the bound density of nanoparticles with high receptor density due to firm adhesion of particles to the wall surface compared to nanoparticles with low receptor density which can be explained by weak adhesive forces, under the same physical condition.

In summary, the coupled particulate and continuum model provides a better understanding of the complex nanoparticle drug delivery process and a design tool to improve nanoparticle targeted delivery efficacy. This model can be used to evaluate multiple physical and chemical parameters to design nanoparticle drug delivery vehicles.

4.2 Future work: evaluation of targeted drug delivery in tumors

In our current work we have coupled the particulate model and continuum model with focus on detachment rate. The detachment rate obtained from the particulate model is coupled with the continuum model to determine the bound density of nanoparticles of various sizes. The future work of this research is to study the complete process which involves simultaneous adhesion and detachment of particles to mimic the actual *in vivo* reaction process. Preliminary result of this idea is illustrated in figure 26.

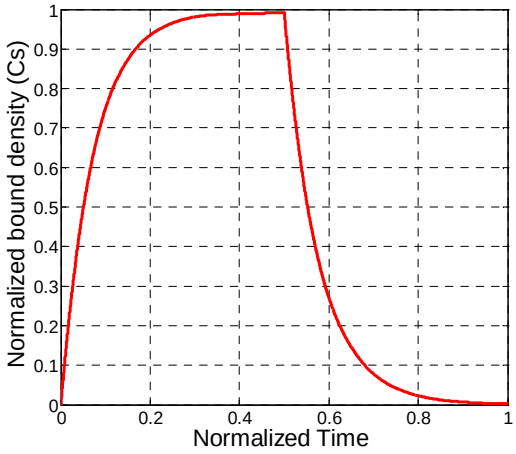

Figure 26 Nanoparticle adhesion dynamic reaction process

Another prospect of future work of this research is tumor drug delivery. Tumor vessels are known to be poorly perfused with blood which limit the delivery of blood based compounds to the tumors. The tumors have abnormal structure associated with the tumor endothelium which leads to the leakiness of the vessel[82]. Thus tumor vessel walls, due to larger gaps, allow particles of larger diameter to leak into the interstitum. An advanced model considering the porosity of the tumor will be developed. To mimic the real vascular geometry, the vascular environment will be reconstructed from CT/MRI images. The multiscale continuum model will be developed to address the physics and chemical reactions involved at the nanoscale. Model predictions will be validated against experimental and clinical data from designed experiments.

Solid tumors are known to have elevated fluid pressure due to high vessel permeability, low lymphatic drainage, poor perfusion and high cell density around blood vessel. Another challenge in tumor drug delivery is tumor interstitial fluid pressure[83] [84] [85]. Jain et al [86] have conducted extensive research effect of interstitial fluid pressure on delivering therapeutic agents to solid tumors. Jain et al [86] conducted *in vivo* experiments to measure interstitial fluid pressure in breast cancer tumors by isolating a tumor connected to blood circulation by a single artery and a single vein. They observed that in normal breast tissue the normal pressure was 8 mmHg while in the breast carcinomas the pressure was 13 mmHg. Due to the high interstitial

pressure, the blood flow is diverted away from the center of the tumor toward a peripheral path leaving a scarcely perfused area in the middle of the tumor[85]. This high interstitial fluid pressure may lower nanoparticle intravasion into the tumors. Since the transport of nanoparticles occurs primarily by convection diffusion process, the transport of nanoparticles in the center region of the tumor may be less than in the tumor periphery. An advanced model accounting for hemodynamics in tumor region will be developed. Thus, the ultimate goal of this study would be to design personalized drug delivery system for patient specific vascular network. This is would help us to design nanoparticles for maximal targeting efficiency and minimal drug dosage to reduce any risk of damaging surrounding cells and reduce overall health care cost.

4.3. Perfusion of DIEP flap

The CFD simulations will help us in choosing proper size of the tissue required for successful transplant and perfusion of the flap after mastectomy. The advantage of such a model is, it eliminates the need to conduct *in vivo* tests which require surgical operations sacrificing the human tissue. We have developed a continuum model to analyze the effect of size, number and interconnectivity of perforators to determine the perfusion in the vascular network. It has been demonstrated that the resistance in small vessels is critical factor than the arterial resistance in deciding the total resistance in the vasculature. The effect of interconnectivity of the vessels has also been evaluated. From our model it can be concluded that using a single large perforator instead of multiple will result in better perfusion of the flap. To account for the resistance in the vasculature, if we don't consider linking vessel, adding a second perforator significantly decreases the network resistance and increased perfusion in the network. However, by considering the linking vessel effect, additional perforator would only increase the perfusion slightly. Thus ligating one perforator will not significantly influence the flow in system with linking vessel. Our results also support the observations made by surgeons.

4.4. Future work: MRI/CT image reconstruction

Beside simple idealized vascular geometry, a realistic model based on MRI/CT images will be developed in the future. The CT/MRI image data is imported to a powerful segmentation tool which converts images to 2D or 3D materialize image format for further analysis. Thresholding the images is first performed to obtain a segmentation mask. We can define a particular range of gray value (pixel range) to obtain region of interest, then region growing is carried out to eliminate noise and separate the structures that are not connected. Finally the materialistic images are exported to standard finite element compatible format. To mimic the real geometry of the vasculature, vascular geometry from MRI/CT image will be exported to the computational environment. To support this idea, an initial result of reconstructed branched vessel is shown in figure 27. A fully established computational model of the DIEP flap will provide enormous opportunity of studying different types of perforator configurations theoretically and characterize its perfusion without bothering to study it clinically.

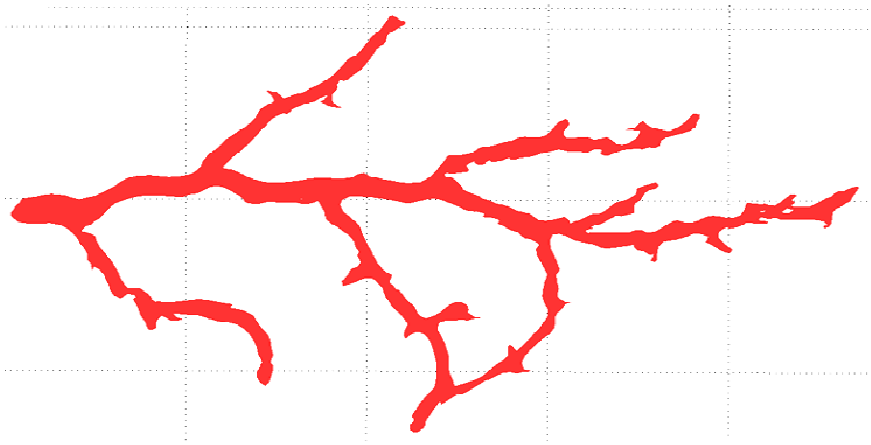

Figure 27 Vascular geometry reconstructed based on MRI image

APPENDIX A

MESH USED IN SIMULATION

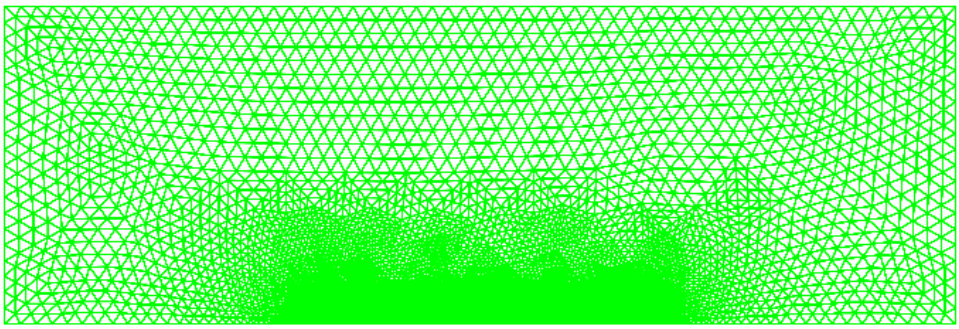

(a)

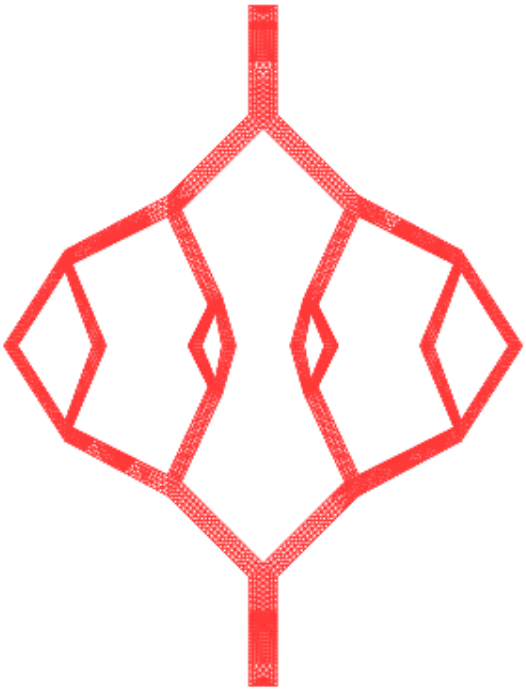

(b)

A 1: Meshes of continuum models used in the simulation (a) Continuum model :number of degrees of freedom solved: 50006 and elements: 24304 (b) Injured blood vessel model: number of elements: 6254 and degrees of freedom solved: 45585.

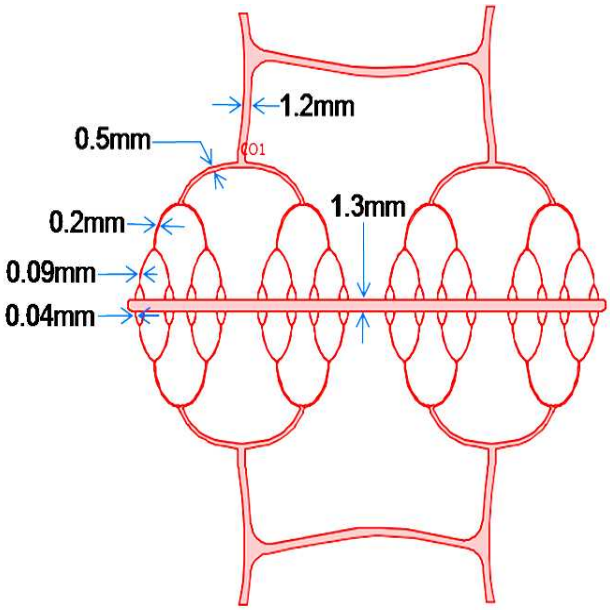

(a)

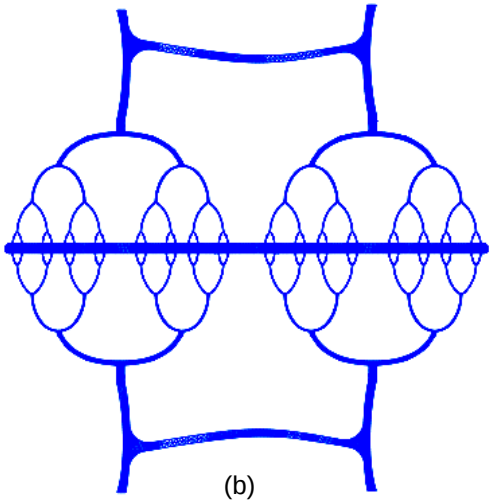

(b)

A 2: Mesh and dimensions of DIEP flap continuum model used in the simulation (a) Continuum model dimensions (b) DIEP flap continuum model: number of elements:57878 and degrees of freedom solved: 298418.

APPENDIX B

VASCULAR GEOMETRY RECONSTRUCTION BASED ON MRI/CT IMAGES

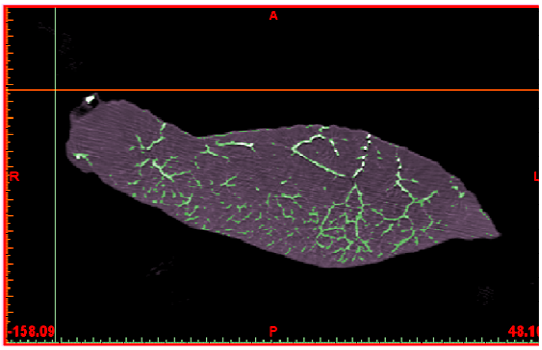

(a)

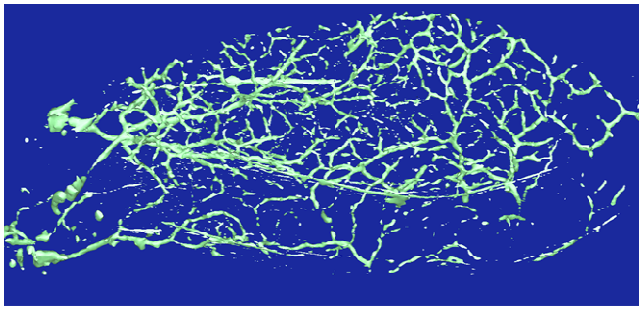

(b)

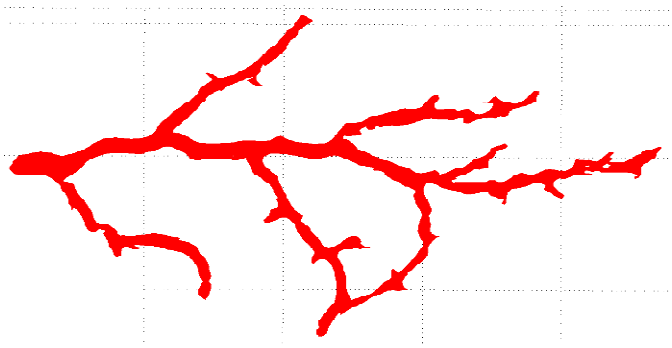

(c)

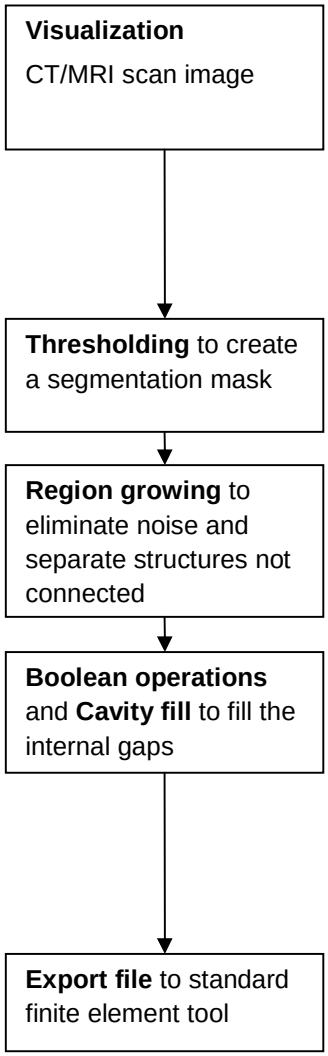

B 1: Process of image reconstruction of DIEP flap

(a) MRI tissue image with vasculature data

(b) Reduced model (c) Final extracted computational model

APPENDIX C

CALCULATION OF NORMALIZED BOUND DENSITY

Physically, the bound density means the number of particles deposited on the target region per unit area and it is mainly governed by the chemical reaction. Another parameter named normalized binding rate is used. First, the bound density of particles on the target region is calculated from the continuum model by integrating number of particles over the target boundary. Then, the following equation is used to calculate the normalized bound density (NBD):

$$NBD = \frac{\text{number of particles deposited under a particular velocity}}{\text{number of particles deposited under static state}}$$

The results for a 500nm nanoparticle have been summarized in following table:

Shear Rate (Dyne/cm^2)	Experimental Bound Density (mol/m^2)	Continuum Bound Density (mol/m^2)
0	0.1	0.1
50	0.05	0.038
70		0.034
100	0.025	0.028
130		0.023
150		0.020
200		0.014
230		0.011
250	0.01	0.009

REFERENCES

1. Wong, C., et al., *Three- and Four-Dimensional Computed Tomography Angiographic Studies of Commonly Used Abdominal Flaps in Breast Reconstruction.* Plastic and Reconstructive Surgery, 2009. **124**(1): p. 18-27 10.1097/PRS.0b013e3181aa0db8.

2. Granzow, J.W., et al., *Breast reconstruction using perforator flaps.* Journal of Surgical Oncology, 2006. **94**(6): p. 441-454.

3. *http://authors.ck12.org/wiki/index.php/Capillaries_-Student_Edition_(Human_Biology)*.

4. Gelperina, S., et al., *The Potential Advantages of Nanoparticle Drug Delivery Systems in Chemotherapy of Tuberculosis.* Am. J. Respir. Crit. Care Med., 2005. **172**(12): p. 1487-1490.

5. Cédric Chauvierre, D.L., Patrick Couvreur and Christine Vauthier, *Novel Polysaccharide-Decorated Poly(Isobutyl Cyanoacrylate) Nanoparticles* Pharmaceutical Research, 2003. **20**(Volume 20): p. 1786-1793.

6. Farokhzad, O.C. and R. Langer, *Nanomedicine: Developing smarter therapeutic and diagnostic modalities.* Advanced Drug Delivery Reviews, 2006. **58**(14): p. 1456-1459.

7. Mathiowitz, E., et al., *Biologically erodable microspheres as potential oral drug delivery systems.* Nature, 1997. **386**(6623): p. 410-414.

8. Jarzyna, P.A., et al., *Multifunctional imaging nanoprobes.* Wiley Interdisciplinary Reviews: Nanomedicine and Nanobiotechnology, 2010. **2**(2): p. 138-150.

9. Roney, C., et al., *Targeted nanoparticles for drug delivery through the blood-brain barrier for Alzheimer's disease.* Journal of Controlled Release, 2005. **108**(2-3): p. 193-214.

10. Sukhorukov, G.B. and H. Möhwald, *Multifunctional cargo systems for biotechnology.* Trends in Biotechnology, 2007. **25**(3): p. 93-98.

11. Hui, N.C.P., *Nanomedicine and Cancer.* 2005.

12. Sawhney, A.S., C.P. Pathak, and J.A. Hubbell, *Bioerodible hydrogels based on photopolymerized poly(ethylene glycol)-co-poly(.alpha.-hydroxy acid) diacrylate macromers.* Macromolecules, 1993. **26**(4): p. 581-587.

13. Moghimi, S.M., A.C. Hunter, and J.C. Murray, *Long-Circulating and Target-Specific Nanoparticles: Theory to Practice.* Pharmacological Reviews, 2001. **53**(2): p. 283-318.

14. Chithrani, B.D., A.A. Ghazani, and W.C.W. Chan, *Determining the Size and Shape Dependence of Gold Nanoparticle Uptake into Mammalian Cells.* Nano Letters, 2006. **6**(4): p. 662-668.

15. Stephanie E. A. Gratton, P.A.R., Patrick D. Pohlhaus, J. Christopher Luft, Victoria J. Madden, Mary E. Napier and Joseph M. DeSimone, *The effect of particle design on cellular internalization pathways.* Proceedings of the National Academy of Sciences of the United States of America, 2008. **105**(33): p. 11613-11618.

16. Jiang, W., et al., *Nanoparticle-mediated cellular response is size-dependent.* Nat Nano, 2008. **3**(3): p. 145-150.

17. YAN GENG, P.D., SHENSHEN CAI, RICHARD TSAI,MANORAMA TEWARI,TAMARA MINKO and DENNIS E. DISCHER, *Shape effects of filaments versus spherical particles in flow and drug delivery.* PubMed Central, 2007: p. 249-255.

18. Champion, J.A., Y.K. Katare, and S. Mitragotri, *Particle shape: A new design parameter for micro- and nanoscale drug delivery carriers.* Journal of Controlled Release, 2007. **121**(1-2): p. 3-9.

19. Ke Zhang, H.F., Zhiyun Chen, John-Stephen A. Taylor, and Karen L. Wooley, *Shape effects of nanoparticles conjugated with cell-penetrating peptides (HIV Tat PTD) on CHO cell uptake.* PubMed Central, 2008.

20. N'Dri, N.A., W. Shyy, and R. Tran-Son-Tay, *Computational Modeling of Cell Adhesion and Movement Using a Continuum-Kinetics Approach.* Biophysical Journal, 2003. **85**(4): p. 2273-2286.

21. F. Gentile , A.G., M. Ferrari , P. Decuzzi, *ON THE ADHESION OF PARTICLES TO A CELL LAYER UNDER FLOW.* 2006.

22. Takalkar, A.M., et al., *Binding and detachment dynamics of microbubbles targeted to P-selectin under controlled shear flow.* Journal of Controlled Release, 2004. **96**(3): p. 473-482.

23. Haun, J.B. and D.A. Hammer, *Quantifying Nanoparticle Adhesion Mediated by Specific Molecular Interactions.* Langmuir, 2008. **24**(16): p. 8821-8832.

24. Moghimi, S.M., A.C. Hunter, and J.C. Murray, *Nanomedicine: current status and future prospects.* FASEB J., 2005. **19**(3): p. 311-330.

25. James R. Heath, M.E.D.a.L.H., *Nanomedicine Targets Cancer.* Scientific American, 2009.

26. Arifin, D.Y., L.Y. Lee, and C.-H. Wang, *Mathematical modeling and simulation of drug release from microspheres: Implications to drug delivery systems.* Advanced Drug Delivery Reviews, 2006. **58**(12-13): p. 1274-1325.

27. Grief, A.D. and G. Richardson, *Mathematical modelling of magnetically targeted drug delivery.* Journal of Magnetism and Magnetic Materials, 2005. **293**(1): p. 455-463.

28. Frieboes, H., et al., *Nanotechnology in Cancer Drug Therapy: A Biocomputational Approach*. 2006. p. 435-460.

29. Glaser, R.W., *Antigen-Antibody Binding and Mass Transport by Convection and Diffusion to a Surface: A Two-Dimensional Computer Model of Binding and Dissociation Kinetics.* Analytical Biochemistry, 1993. **213**(1): p. 152-161.

30. Bell, G., *Models for the specific adhesion of cells to cells.* Science, 1978. **200**(4342): p. 618-627.

31. Evans, E.A., *Detailed mechanics of membrane-membrane adhesion and separation. II. Discrete kinetically trapped molecular cross-bridges.* Biophysical Journal, 1985. **48**(1): p. 185-192.

32. Lopez-Otin, C. and E.P. Diamandis, *Breast and Prostate Cancer: An Analysis of Common Epidemiological, Genetic, and Biochemical Features.* Endocr Rev, 1998. **19**(4): p. 365-396.

33. Figus, A., V. Ramakrishnan, and C. Rubino, *Hemodynamic Changes in the Microcirculation of DIEP Flaps.* Annals of Plastic Surgery, 2008. **60**(6): p. 644-648 10.1097/SAP.0b013e318145be31.

34. Rubino, C., et al., *Haemodynamic enhancement in perforator flaps: The inversion phenomenon and its clinical significance. A study of the relation of blood velocity and flow between pedicle and perforator vessels in perforator flaps.* Journal of Plastic, Reconstructive & Aesthetic Surgery, 2006. **59**(6): p. 636-643.

35. de Weerd, L., Å.O. Miland, and J.B. Mercer, *Perfusion Dynamics of Free DIEP and SIEA Flaps During the First Postoperative Week Monitored With Dynamic Infrared Thermography.* Annals of Plastic Surgery, 2009. **62**(1): p. 42-47 10.1097/SAP.0b013e3181776374.

36. Patel, S.A. and A. Keller, *A theoretical model describing arterial flow in the DIEP flap related to number and size of perforator vessels.* Journal of Plastic, Reconstructive & Aesthetic Surgery, 2008. **61**(11): p. 1316-1320.

37. Dobson, J., *Magnetic nanoparticles for drug delivery.* Drug Development Research, 2006. **67**(1): p. 55-60.

38. Decuzzi, P. and M. Ferrari, *The adhesive strength of non-spherical particles mediated by specific interactions.* Biomaterials, 2006. **27**(30): p. 5307-5314.

39. Decuzzi, P. and M. Ferrari, *Design maps for nanoparticles targeting the diseased microvasculature.* Biomaterials, 2008. **29**(3): p. 377-384.

40. Won, J., et al., *Diffusion of Spheres in Entangled Polymer Solutions: A Return to Stokes-Einstein Behavior.* Macromolecules, 1994. **27**(25): p. 7389-7396.

41. Silberzan, J.B.a.P., *Microfluidics for Biotechnology.* Artech House microelectromechanical systems series, Microelectromechanical systems series, 2006.

42. Hyun J. Kwon, C.K.B., Brian T. Dodge, and George S. Agoki, *Study of Simultaneous Fluid and Mass Adsorption Model in the QCM-D Sensor for Characterization of Biomolecular Interactions.* COMSOL Conference 2009 Boston.

43. Stokholm, R., et al., *Determination of Wall Shear Rate in the Human Carotid Artery by Magnetic Resonance Techniques.* European Journal of Vascular and Endovascular Surgery, 2000. **20**(5): p. 427-433.

44. Wu, S.P., et al., *Wall shear rates differ between the normal carotid, femoral, and brachial arteries: An in vivo MRI study.* Journal of Magnetic Resonance Imaging, 2004. **19**(2): p. 188-193.

45. Stroev, P.V., P.R. Hoskins, and W.J. Easson, *Distribution of wall shear rate throughout the arterial tree: A case study.* Atherosclerosis, 2007. **191**(2): p. 276-280.

46. Kalyanasundaram, S., V.D. Calhoun, and K.W. Leong, *A finite element model for predicting the distribution of drugs delivered intracranially to the brain.* Am J Physiol Regul Integr Comp Physiol, 1997. **273**(5): p. R1810-1821.

47. Goldstein, B. and F.W. Wiegel, *The effect of receptor clustering on diffusion-limited forward rate constants.* Biophysical Journal, 1983. **43**(1): p. 121-125.

48. Erickson, J., et al., *The effect of receptor density on the forward rate constant for binding of ligands to cell surface receptors.* Biophysical Journal, 1987. **52**(4): p. 657-662.

49. Omid C. Farokhzad, A.K., Sangyong Jon, Aurelia Hermmann,Jianjun Cheng, Curtis Chin, Alice Kiselyuk,Benjamin Teply,George Eng and Robert Langer, *Microfluidic System for Studying the Interaction of Nanoparticles and Microparticles with Cells.* Analytical Chemistry, 2005. **77**(17): p. 5453-5459.

50. Ravi A. Vijayendran, F.S.L.a.D.E.L., *A Computational Reaction-Diffusion Model for the Analysis of Transport-Limited Kinetics.* Analytical Chemistry, 1999. **71**: p. 5405-5412.

51. American Cancer Society, C.r.i., Cancer facts and figures 2009.

52. Center, T.U.o.T.M.A.C., *Patient and caner information- Breast Cancer.*

53. Philip N. Blondeel, K.H.I.V.L., Stan J. M. Monstery, Moustapha Hamdi, Guido E. Matton, Robert J. Allen, Charles Dupin, Axel-Mario Feller, Isao Koshlina, Naci Kostakoglu and Fu-Chan Wei, *The "Gent" Consensus on Perforator Flap Terminology : Preliminary*

Definitions. Journal of Plastic, Reconstructive and Aesthetic Surgery, June 2006. **59**(6): p. 571-579.

54. Heitland, R.A.a.A., *Autogenous augmentation mammaplasty with microsurgical tissue transfer.* Journal of Plastic Reconstructive Surgery, 2003. **112**: p. 91-100.

55. Allen, R.J. and P. Treece, *Deep Inferior Epigastric Perforator Flap for Breast Reconstruction.* Annals of Plastic Surgery, 1994. **32**(1): p. 32-38.

56. Futter, C.M., et al., *A retrospective comparison of abdominal muscle strength following breast reconstruction with a free TRAM or DIEP flap.* British Journal of Plastic Surgery, 2000. **53**(7): p. 578-583.

57. Kaplan, J.L. and R.J. Allen, *Cost-Based Comparison between Perforator Flaps and TRAM Flaps for Breast Reconstruction.* Plastic and Reconstructive Surgery, 2000. **105**(3): p. 943-948.

58. Allen, R.J., *Diep Versus Tram for Breast Reconstruction.* Plastic and Reconstructive Surgery, 2003. **111**(7): p. 2478.

59. Jay W. Granzowa, J.L.L., Ernest S. Chiub and Robert J. Allen, *Breast Reconstruction with the Deep Inferior Epigastric Perforator Flap: History and an update on current technique.* Journal of Plastic, Reconstructive & Aesthetic Surgery, 2006. **59**(6): p. 571-579.

60. Gill, P.S., et al., *A 10-Year Retrospective Review of 758 DIEP Flaps for Breast Reconstruction.* Plastic and Reconstructive Surgery, 2004. **113**(4): p. 1153-1160 10.1097/01.PRS.0000110328.47206.50.

61. Rubino C, C.V., Cavazzuti AM, Canu V, *Haemodynamic enhancement in perforator flaps:The inversion phenomenon and its clinical significance. A study of the relation of*

blood velocity and flow between pedicle and perforator vessels in perforator flaps. Journal of Plastic Reconstructive and Aesthetic Surgery, 2005: p. 636-643.

62. Coscia, V. and C. Rubino, *Hemodynamic enhancement in reconstructive surgery: Mathematical model and clinical findings.* Mathematical and Computer Modelling, 2005. **42**(9-10): p. 1151-1161.

63. Klabunde, R.E., *Determinants of Resistance to flow (Poiseuille's Equation).*

64. Jurczuk, K. and M. Krętowski, *Parallel Implementation of Vascular Network Modeling*. 2008. p. 679-688.

65. *Tranlating blood pressure numbers.* http://www.new-fitness.com/Blood_Pressure/numbers.html.

66. Cutnell, J.J., Kenneth., Wiley Physics, 1998. **308 Fourth Edition**.

67. Késmárky, G., et al., *Plasma viscosity: A forgotten variable.* Clinical Hemorheology and Microcirculation, 2008. **39**(1): p. 243-246.

68. Anor, T., et al., *Modeling of blood flow in arterial trees.* Wiley Interdisciplinary Reviews: Systems Biology and Medicine, 2010. **9999**(9999): p. n/a.

69. Formaggia, L., et al., *Numerical modeling of 1D arterial networks coupled with a lumped parameters description of the heart.* Computer Methods in Biomechanics and Biomedical Engineering, 2006. **9**(5): p. 273 - 288.

70. Mabotuwana, T., L. Cheng, and A. Pullan, *A model of blood flow in the mesenteric arterial system.* BioMedical Engineering OnLine, 2007. **6**(1): p. 17.

71. Alastruey, J., et al., *Reduced modelling of blood flow in the cerebral circulation: Coupling 1-D, 0-D and cerebral auto-regulation models.* International Journal for Numerical Methods in Fluids, 2008. **56**(8): p. 1061-1067.

72. Westerhof, N., J.-W. Lankhaar, and B.E. Westerhof, *The arterial Windkessel.* Medical & Biological Engineering & Computing, 2009. **47**(2): p. 131-141.

73. Segers, P., et al., *Pulmonary arterial compliance in dogs and pigs: the three-element windkessel model revisited.* Am J Physiol Heart Circ Physiol, 1999. **277**(2): p. H725-731.

74. Kumar, B.V.R., et al., *On parallel computation of blood flow in human arterial network based on 1-D modelling.* Computing, 2003. **71**(4): p. 321-351.

75. *http://en.wikipedia.org/wiki/Artery.*

76. *http://library.thinkquest.org/C0115080/?c=vessels#arteries.*

77. *http://www.dimensionsguide.com/blood-vessels-diameter/.*

78. Jean Hopkins, C.W.M., Susan Johnson, Maryanna Quon Warner, David LaHart, Jill D. Wright, *Human Biology and Health.* 1993.

79. *www.ehow.com.*

80. *http://science.jrank.org/pages/1181/Capillaries.html.* **http://www.ehow.com/video_4790458_how-many-blood-vessels-human.html**.

81. Andrea Lionello, J.J., Henrik Jensen and Hubert H. Girault, *Dynamic protein adsorption in microchannels by ''stop-flow'' and continuous flow.* The Royal Society of Chemistry, 2005. **5**: p. 1096-1103.

82. R.K.Jain, *Barriers to drug delivery in Solid tumors.* Scientific American, 1994. **271**: p. 58-65.

83. Stephane Ferretti, P.R.A., Mike M. Becquet and Paul M.J. McSheehy, *Tumor Interstitial Fluid Pressure as an Early-Response Marker for Anticancer Therapeutics.* NEO PLASIA, 2009. **11**(9): p. 874-881.

84. Netti, P.A., et al., *Effect of Transvascular Fluid Exchange on Pressure-Flow Relationship in Tumors: A Proposed Mechanism for Tumor Blood Flow Heterogeneity.* Microvascular Research, 1996. **52**(1): p. 27-46.

85. Mollica, F., R.K. Jain, and P.A. Netti, *A model for temporal heterogeneities of tumor blood flow.* Microvascular Research, 2003. **65**(1): p. 56-60.

86. Jain, R.K., *Delivery of molecular and cellular medicine to solid tumors.* Journal of Controlled Release, 1998. **53**(1-3): p. 49-67.

BIOGRAPHICAL INFORMATION

Manohara Mariyappa graduated with a Bachelor of Engineering degree in Mechanical Engineering from Visvesvaraya Technological University, India in June 2005. After completing his Bachelor's, he worked as a Project Engineer at Wipro Technologies India from July 2005 to July 2007. He began his Master's program in Mechanical Engineering at University of Texas at Arlington from January 2008. In summer of 2009 he joined Dr. Liu's Bio-nanomechanics lab and worked on research projects, mainly dealing with computational modeling of biological systems.

Manohara Mariyappa received his master's degree in mechanical engineering from The University of Texas at Arlington in May 2010.